

Warsaw University of Technology

FACULTY OF
POWER AND AERONAUTICAL ENGINEERING



Institute of Aeronautics and Applied Mechanics

Bachelor's diploma thesis

in the field of study Aerospace Engineering
and specialisation Aerospace Engineering

Design and aerodynamic analysis of a ground effect sports car

Rafał Szulejko

student record book number 271093

thesis supervisor
Janusz Piechna, PhD. Sc

Warsaw, 2021

Abstract

Ground effects were introduced in motorsport in late 1960s and continue to be the most regulated aerodynamic component in motorsport. Every significant improvement in this area caused an uncompetitive racing season and have been subsequently banned by the series regulating body, with the sole exception of widely adopted deep Venturi tunnels in the 1980s and early 1990s Group C endurance prototypes. Current open wheel and endurance prototype regulations stipulate the use of flat floor and diffusers starting around the rear axle in order to closely limit the created downforce. Recent developments in this area include Brabham BT46B-inspired suction fan implemented by Adrian Newey (Red Bull X2010) and Gordon Murray (GMA T.50), as well as Venturi tunnels applied on the previously unseen scale in Newey's Aston Martin Valkyrie. All three were designed with no respect to any racing regulations and promise performance impossible to achieve with conventional methods. This project aims to design, implement and simulate the similar approach to the Aston Martin Valkyrie, with the exception of a different front aerodynamic device, specifically the Formula One-inspired front wing replaced by two large separate Venturi tunnels surrounding the front of the tub.

Keywords: CFD, motorsport, ground effect, automotive, car, aerodynamics, ground effect

Streszczenie

Efekty przypowierzchniowe zostały wprowadzone do sportów motorowych w późnych latach sześćdziesiątych i od tego czasu pozostają najbardziej rygorystycznie uregulowanym elementem aerodynamicznym samochodów wyścigowych. Wszystkie znaczące innowacje w tym obszarze powodowały dominację jednego zespołu oraz niemal natychmiastowy zakaz jej stosowania w przyszłych sezonach wprowadzony przez organy regulacyjne, za wyjątkiem długodystansowych prototypów Grupy C z lat osiemdziesiątych i wczesnych dziewięćdziesiątych, gdzie głębokie tunele Venturiego zostały zastosowane przez całą stawkę. Wszystkie obecne regulacje długodystansowych prototypów oraz samochodów wyścigowych z otwartym nadwoziem wymagają stosowania płaskiej podłogi i dyfuzora zaczynającego się w okolicach tylnej osi. Ostatnie prace rozwojowe w obszarze samochodowych efektów przypowierzchniowych opierają się na wykorzystaniu wentylatora zasysającego powietrze nawiązującego do Brabham GT46B (Adrian Newey - Red Bull X2010, Gordon Murray - GMA T.50), a także użyciu tuneli Venturiego na niespotykanej dotychczas skalę (Adrian Newey - Aston Martin Valkyrie). Wszystkie trzy wymienione projekty zostały zaprojektowane bez odniesienia do istniejących technicznych regulacji w motorsporcie. Celem tej pracy jest zaprojektowanie, zastosowanie oraz analiza rozwiązania inspirowanego Valkyrie, ze zmienionym przednim elementem aerodynamicznym - dodatkowe tunele Venturiego zamiast wielopłatowego skrzydła w stylu F1.

Słowa kluczowe: CFD, sporty motorowe, motoryzacja, aerodynamika, efekt przyziemny, samochód

Oświadczenie autora (autorów) pracy

Świadomy/-a odpowiedzialności karnej za składanie fałszywych zeznań oświadczam, że niniejsza praca dyplomowa została napisana przeze mnie samodzielnie, pod opieką kierującego pracą dyplomową.

Jednocześnie oświadczam, że:

- niniejsza praca dyplomowa nie narusza praw autorskich w rozumieniu ustawy z dnia 4 lutego 1994 roku o prawie autorskim i prawach pokrewnych (Dz.U. z 2006r. Nr 90, poz. 631 z późn. zm.) oraz dóbr osobistych chronionych prawem cywilnym,
- niniejsza praca dyplomowa nie zawiera danych i informacji, które uzyskałem/-am w sposób niedozwolony,
- niniejsza praca dyplomowa nie była wcześniej podstawą żadnej innej urzędowej procedury związanej z nadawaniem dyplomów lub tytułów zawodowych,
- wszystkie informacje umieszczone w niniejszej pracy, uzyskane ze źródeł pisanych i elektronicznych, zostały udokumentowane w wykazie literatury odpowiednimi odnośnikami,
- znam regulacje prawne Politechniki Warszawskiej w sprawie zarządzania prawami autorskimi i prawami pokrewnymi, prawami własności przemysłowej oraz zasadami komercjalizacji.

Oświadczam, że treść pracy dyplomowej w wersji drukowanej, treść pracy dyplomowej zawartej na nośniku elektronicznym (płycie kompaktowej) oraz treść pracy dyplomowej w module APD systemu USOS są identyczne.

.....
data

.....
podpis autora (autorów) pracy

Oświadczenie

Wyrażam zgodę / nie wyrażam zgody^{*1} na udostępnianie osobom zainteresowanym mojej pracy dyplomowej. Praca może być udostępniana w pomieszczeniach biblioteki wydziałowej. Zgoda na udostępnienie pracy dyplomowej nie oznacza wyrażenia zgody na jej kopowanie w całości lub w części.

Brak zgody nie oznacza ograniczenia dostępu do pracy dyplomowej osób:

- reprezentujących władze Politechniki Warszawskiej,
 - członków Komisji Akredytacyjnych,
 - funkcjonariuszy służb państwowych i innych osób uprawnionych, na mocy odpowiednich przepisów prawnych obowiązujących na terenie Rzeczypospolitej Polskiej, do swobodnego dostępu do materiałów chronionych międzynarodowymi przepisami o prawach autorskich.
- Brak zgody nie wyklucza także kontroli tekstu pracy dyplomowej w systemie antyplagiatowym.

.....
data

.....
podpis autora (autorów) pracy

^{*1} - niepotrzebne skreślić

Table of contents

Abstract	2
Streszczenie	3
Table of contents	5
1. Introduction and history of passive ground effects use in motorsport and performance road cars.....	6
1.1. Scope of the thesis	6
1.2. Race cars	6
1.3. Road cars	8
2. Design	10
2.1. Initial design and aerodynamic approach.....	10
2.2. Shift in front aerodynamic design.....	11
2.3. Floor design.....	12
2.4. Notable design elements	13
3. CAD model	14
3.1. Iterative approach	14
3.2. Bodywork.....	15
4. CFD setup	17
4.1. Mesh and boundary conditions	17
4.2. Models, methods and solver setup	19
5. CFD results.....	20
5.1. Convergence, quantitative results and validation	20
5.2. Initial pressure plots analysis	21
5.3. Detailed flow analysis	26
5.4. SAS transient analysis.....	34
6. Conclusions	37
Bibliography	38
List of figures	39

1. Introduction and history of passive ground effects use in motorsport and performance road cars

1.1. Scope of the thesis

The following project involves design, CAD modeling and CFD analysis of a car loosely inspired by the Aston Martin Valkyrie and several other modern design approaches. The basic design and initial design estimation were based around known Aston Martin Valkyrie dimensions as well as standard 2D human manikin. Then the 3D CAD design was created in Siemens NX software, which was later meshed and used in ANSYS Fluent simulation. The last and major part of this thesis is dedicated to analysis of the results and explanation of physical phenomena behind them. In order to achieve this, multitude of contour and pathline plots were used.

1.2. Race cars

While any attempt of active ground effects use (Figure 1) was quickly banned by the regulators, passive and semi-passive enjoyed a longer stint in a form of open wheel (Lotus 78 to 88, Chaparral 2K) and most prominently, Group C endurance prototypes, of which Porsche 956/962 family is the most successful.

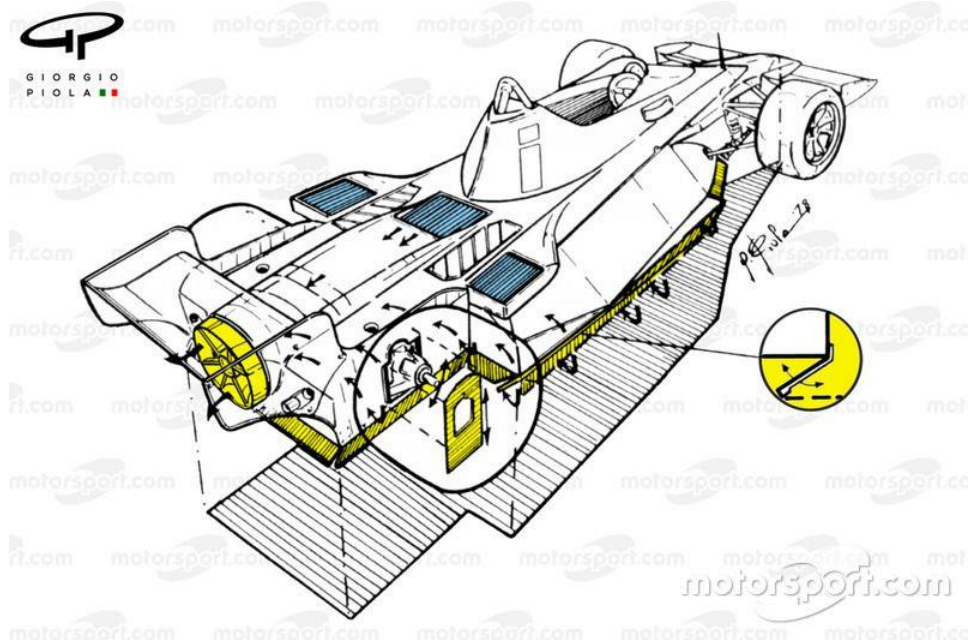


Figure 1: 1978 Brabham BT46B, the second and final fan-based ground effect race car [12]

Ground effects were introduced to Formula 1 by the Colin Chapman-led Lotus team with the 1977-78 '78' model [9]. The car had sidepods shaped into a large airfoil-like shape, which was hidden from the outside using suspension-mounted skirt and brush system to seal the resulting tunnel (Figure 2). The car was the fastest during its debut year and sparked the ground effect revolution in Formula 1 up until the 1983 ban of the ground effects use. During this time, most titles were won using this technology, and success outside F1 include 1980 Chaparral 2K winning Indy 500 and CART Championship.

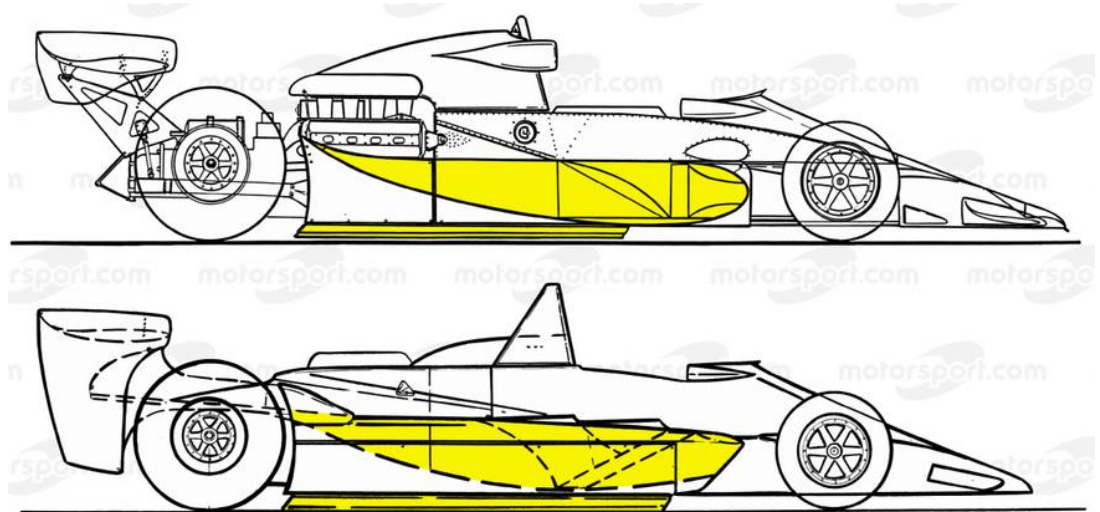


Figure 2: Lotus 78 (top) and 79 (bottom). While 78 was technically a working implementation of the ground effect sidepods, Lotus did not win a championship with ground-effect car before using much-upgraded 79 [9].

Introduction of ground effects into endurance prototypes overlaps with their retirement from open-wheel cars - the most famous and successful example, the Porsche 956 debuted in 1982 [11]. Instead of the sidepods, the cars started using large and deep Venturi tunnels starting near the center of the car's length (Figure 3). Porsche's approach to feeding the tunnels was completely different from the F1 skirt cars though. Lead designer Norbert Singer noted that the breakthrough came when they started feeding the tunnels with the air from the sides, a completely opposite approach from the Lotus' skirts.



Figure 3: Early Porsche 956 aerodynamic model with deep Venturi tunnels visible [11].

The ground effects are being reintroduced into motorsport in a form of 2022 F1 rules, in an effort to decrease dependence on outer aerodynamic devices, which create massive wake of

turbulent air slowing down following cars. Instead of the Lotus 78-like shrouded sidepods, a reshaped floor is used (Figure 4).

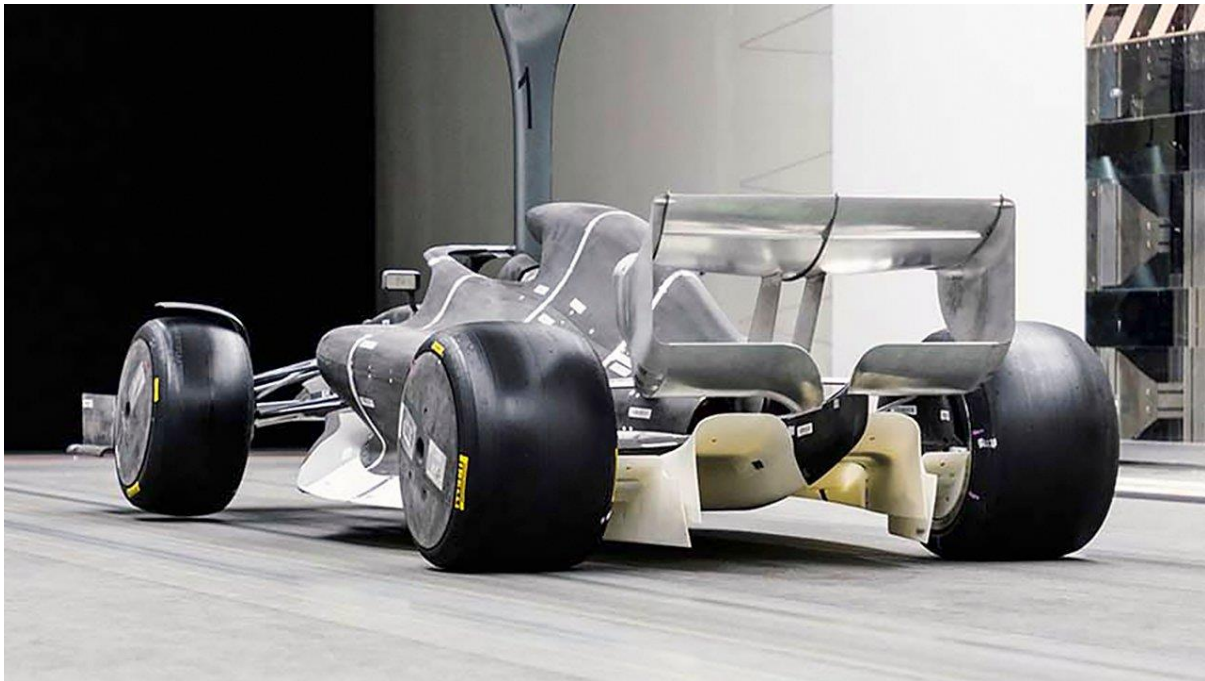


Figure 4: 2022 F1 regulations reference aerodynamic scale model. The new tunnels are white. [5]

1.3. Road cars

Since any use of ground effects was banned up until the 2022 F1 regulations, most of the recent development happened in the area of track-oriented road cars, with the prominent examples of Elemental Rp1 and Aston Martin Valkyrie. Elemental RP1 is a 595 kg two-seat open-top road car that debuted in 2015. It has no wings, and creates 400 kg of downforce at 240 km/h. This is caused by usage of two front Venturi tunnels (Figure 5). This is not the first application of this concept, with the earliest known similar solutions being used since late 1990s in LMP and GT1 endurance prototypes, but it is much more prominent than any other solution and has the biggest influence on the overall car design. Unlike previous regulation-limited approaches it is also opened at the bottom, with the previous cars having floor extended into the tunnels.



Figure 5: Elemental RP1 underfloor. [7]

The latest and most extreme development in the ground effects in performance cars is the Aston Martin Valkyrie, designed by Adrian Newey (Figure 6). The car features a monocoque with the occupants' feet and knees above their thighs, open wheel-style multi-element front wing and Venturi tunnels running across most of the car's length. The front Formula-style double element wing both creates downforce on the front and creates large low-pressure vortices reminiscent of Formula 1 Y250 vortices, that are led into the rear tunnels to become the primary source of the car's downforce. The projected downforce levels are expected to be around 1800 kg as per manufacturer's press release (speed not specified), which is more than double what other manufacturers have shown previously (2018 McLaren Senna produces 800 kg at 250 km/h). This is also without use of a prominent rear wing.



Figure 6: Aston Martin Valkyrie. Visible multi-element front wing and deep tunnels spanning most of the car's length. [2]

2. Design

2.1. Initial design and aerodynamic approach

The basic layout of the vehicle was inspired by Adrian Newey's initial design drawings of the Valkyrie. This involves side-by-side Formula One-style seating with knees above the back, and monocoque closely enveloping the driver and passenger. The other element carried over is focus on large rear tunnels, with the narrow V-layout engine and gearbox being above. To estimate the dimensions and get a reasonable design, various design drawings were done early in the design process. Based on a reference 2D human manikin and Aston Martin Valkyrie design drawing, a sizing model was drawn for future reference (Figure 7, Figure 8).

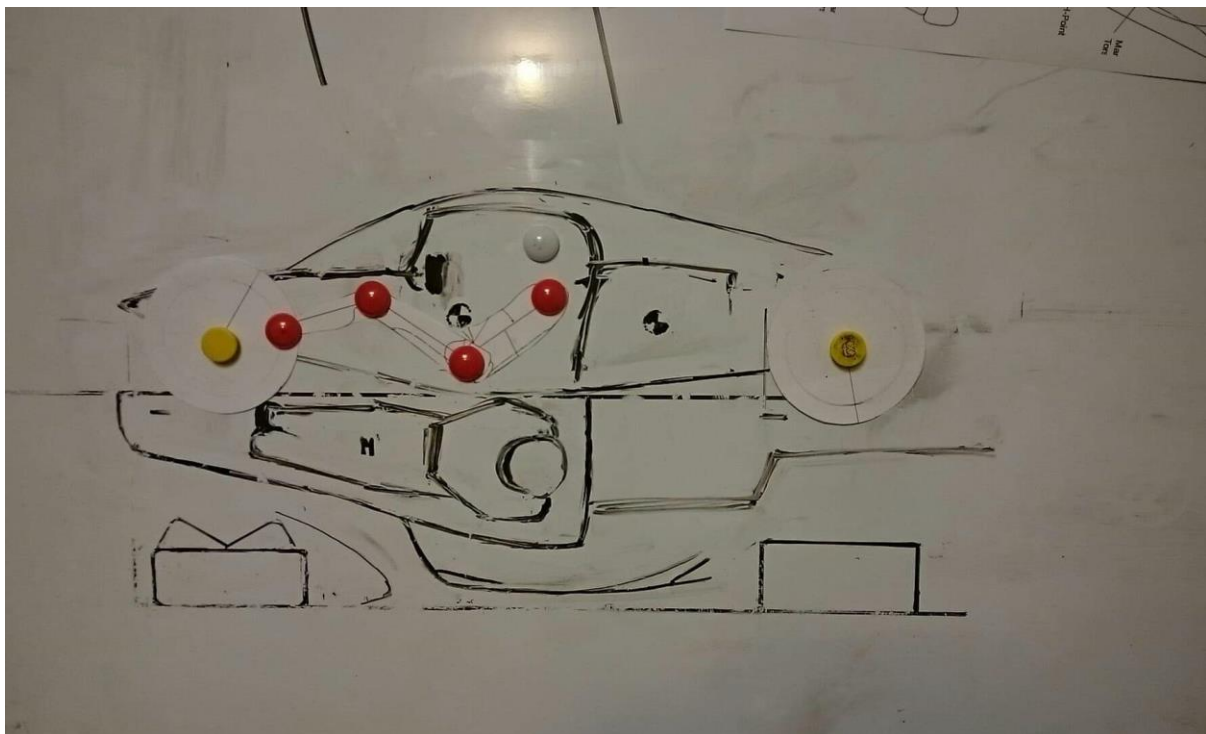


Figure 7: Initial whiteboard drawing with 2D human dummy

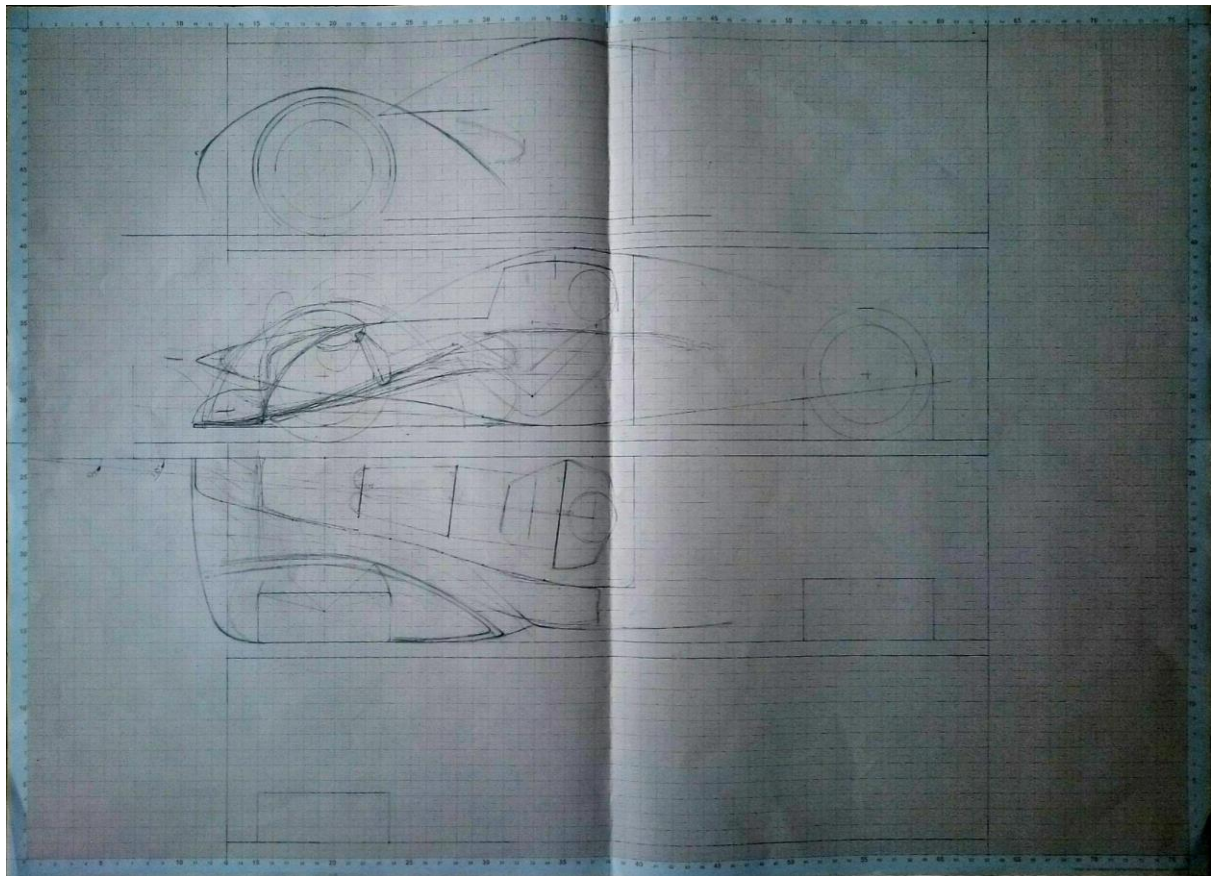


Figure 8: Final design drawing

2.2. Shift in front aerodynamic design

The major shift from the Aston Martin car is in the front aerodynamic devices, with the original car having F1-style multi-element wing and my design having large Venturi tunnels. This change, even though providing downforce around the front axle as well, has far-reaching design implications. The top surface of those tunnels guides the air to the side-mounted radiators and the inner vertical walls guide the air into the rear tunnels (Figure 9).

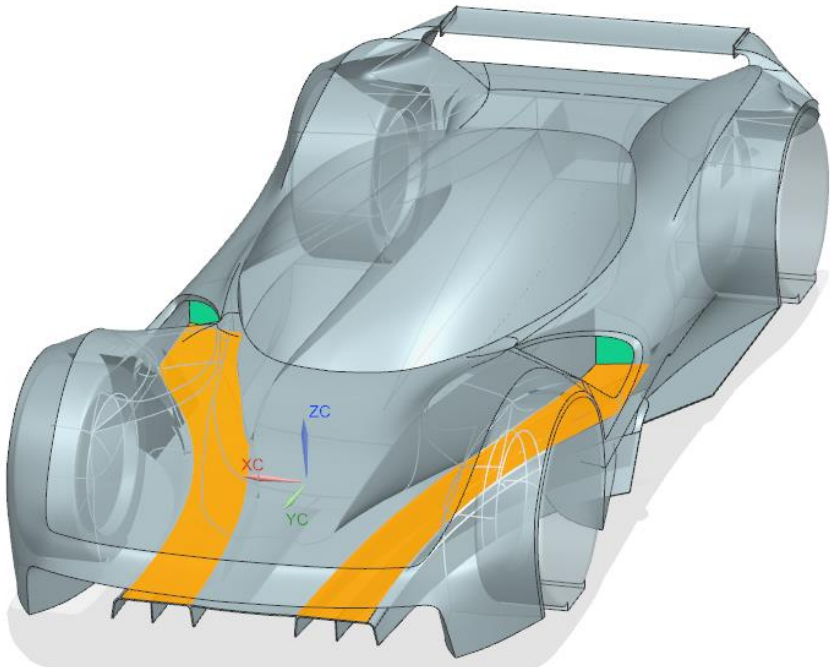


Figure 9: Top surfaces of the front tunnels lead air to the side radiators.

2.3. Floor design

Rear part of the floor is much closer to the RP1 and Valkyrie - the rear tunnels start at the lowest point of the tub and extend up to the end of the rear overhang (Figure 10).

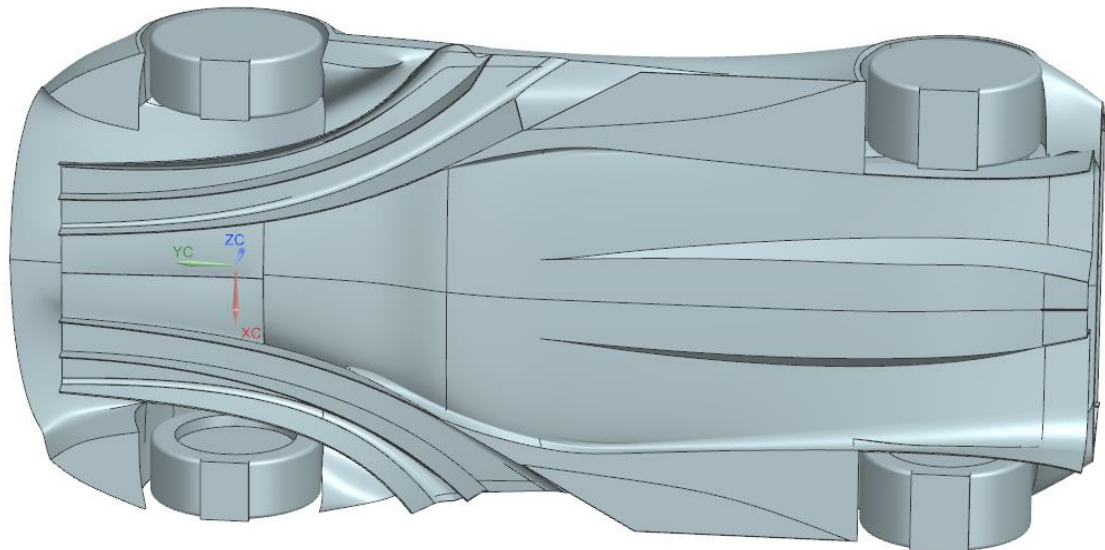


Figure 10: Car's final underfloor design.

2.4. Notable design elements

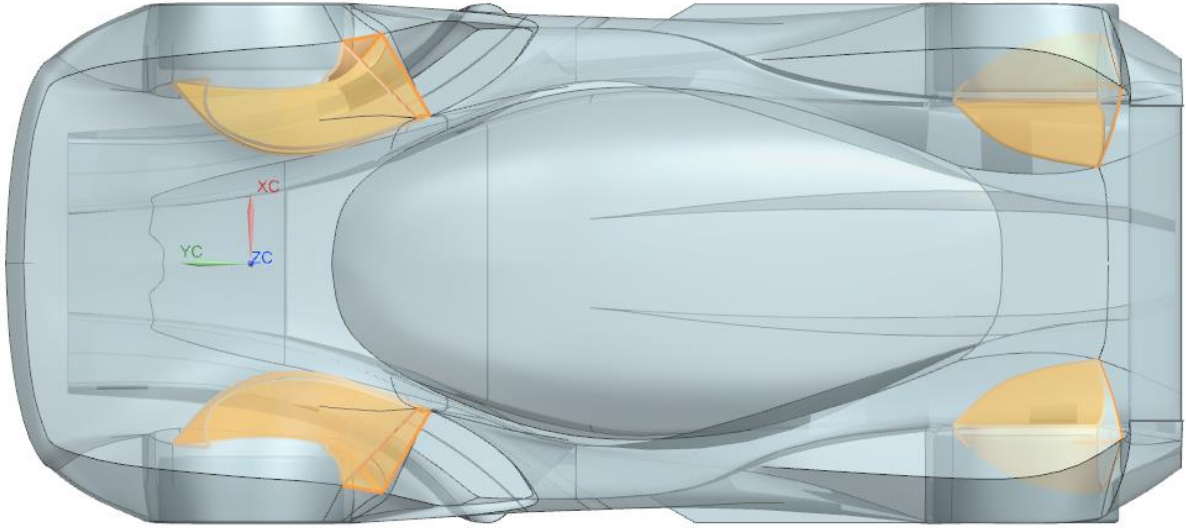


Figure 11: Wheel well pressure outlets highlighted.

Cooling solution was an important part of the design, and simulating radiators with just a wall was too much of a simplification. To simulate the cooling system accurately enough, an internal channel connecting side inlets with rear outlets was added (Figure 12). For further cooling and pressure relief, wheel well outlets were added into the fenders (Figure 11). Loss of downforce caused by increased wheel well pressure was found to be a significant safety threat, and vents were finally mandated to be used in all LMP1 and LMP2 cars since early 2010s. As this was supposed to be a road-legal performance car, the outlets were shaped in a way that the wheel is invisible from the top.

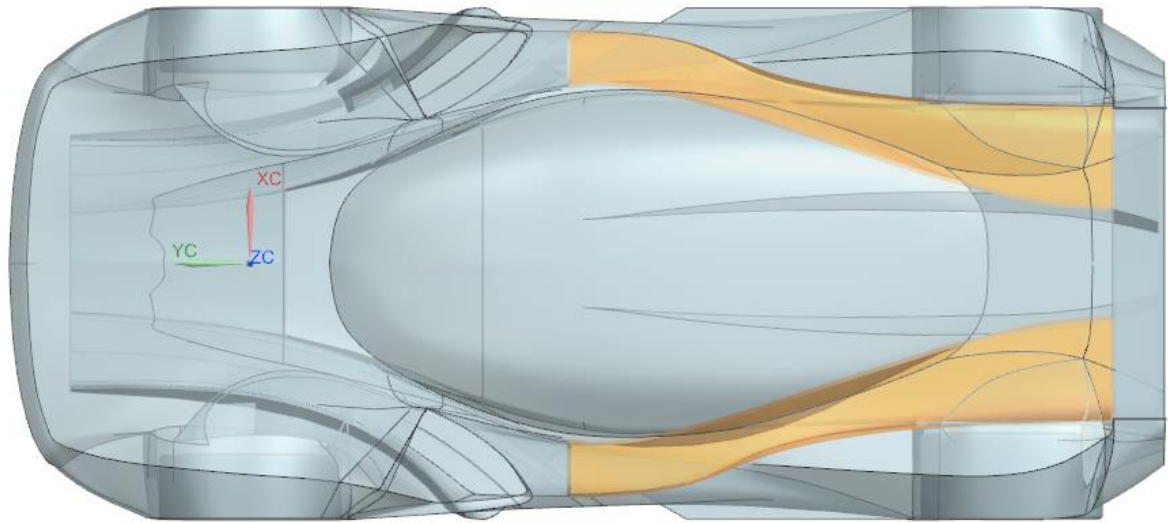


Figure 12: Internal tunnels for cooling system simulation.

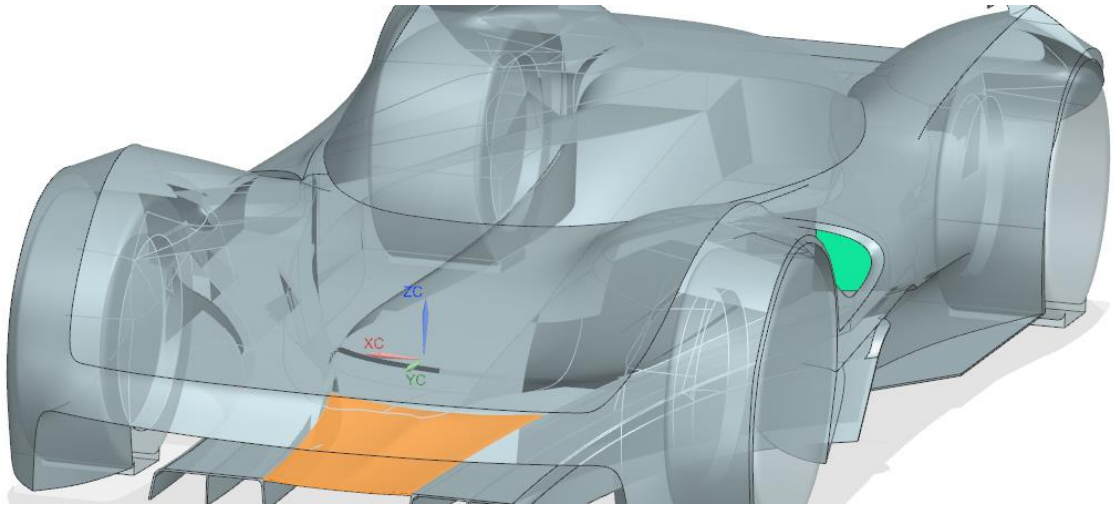


Figure 13: After initial analysis, a surface connecting front tunnels was added.

For the rear wing, Selig's S1223 low-speed high-lift airfoil was used.

3.CAD model

3.1. Iterative approach

The car was modeled entirely using Siemens NX software. The initial design followed basic dimensions specified by drawings, but the drawings provided only outer projected dimensions of the tub, meaning that the resulting model was very spatially inefficient. The new model was made based on the previous one, but more closely enveloping the driver compartment. Then, the front tunnels were remodeled from scratch. The new tunnels were much wider and usage of parameterization allowed for later changes (Figure 14). Then the powertrain mockup and rear tunnels were added. All those components were modeled using conventional NX tools - solid and surface modeling.

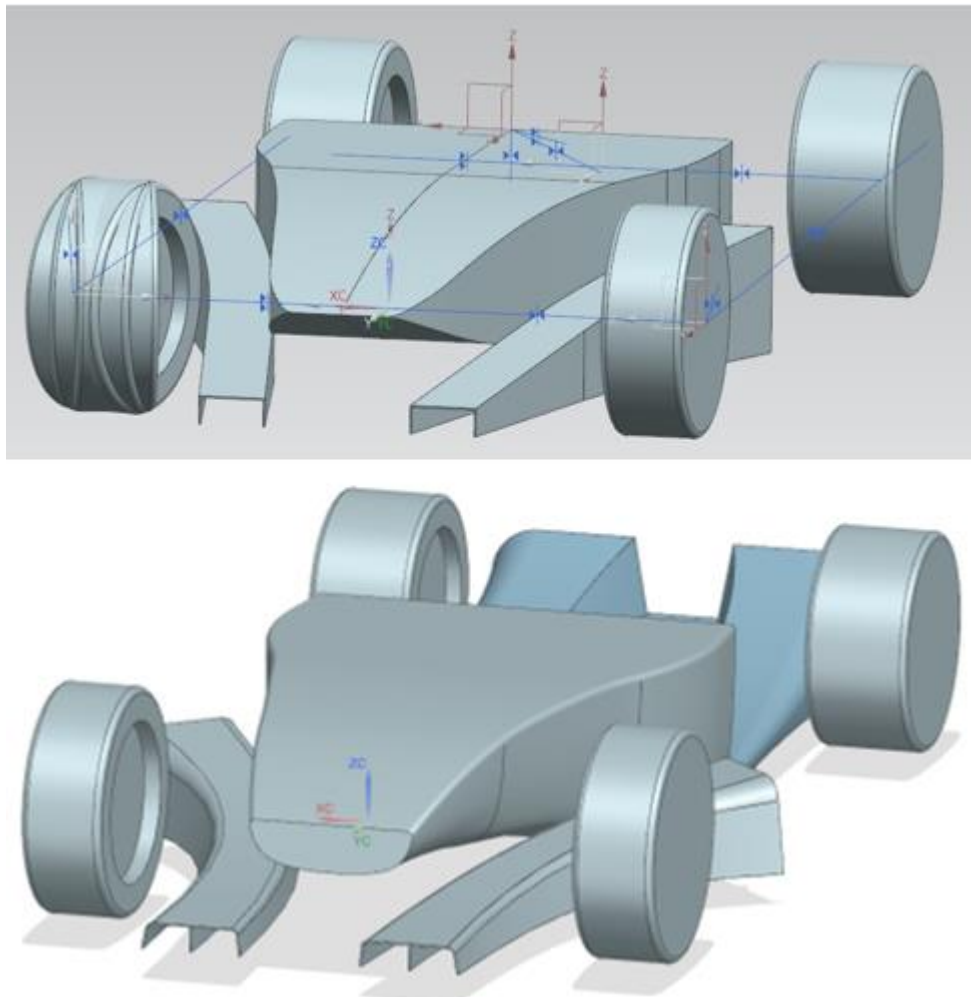


Figure 14: Initial and final versions of tub and front tunnels.

3.2. Bodywork

Due to the high complexity and need for ability to quickly change selected features, the bodywork was modeled using NX Realize Shape freeform modeling module. Traditional surface modeling, where engineers use parametric and constrained splines and then wraps surfaces across these curves, using tools like Sweep and Through Curve Mesh. This allows for highly parametric design and close control over tangency and curvature of resulting surfaces. Realize Shape (also called subdivision modeling) is based around more clay-like modeling, starting with a primitive shape and dragging its cage's vertices and edges across the screen using a mouse. This was later found to be highly problematic as the surfaces generated by the Realize Shape tool are made of small parts that are harder to control and constrain, and that complicates the mesh generation later (Figure 16).

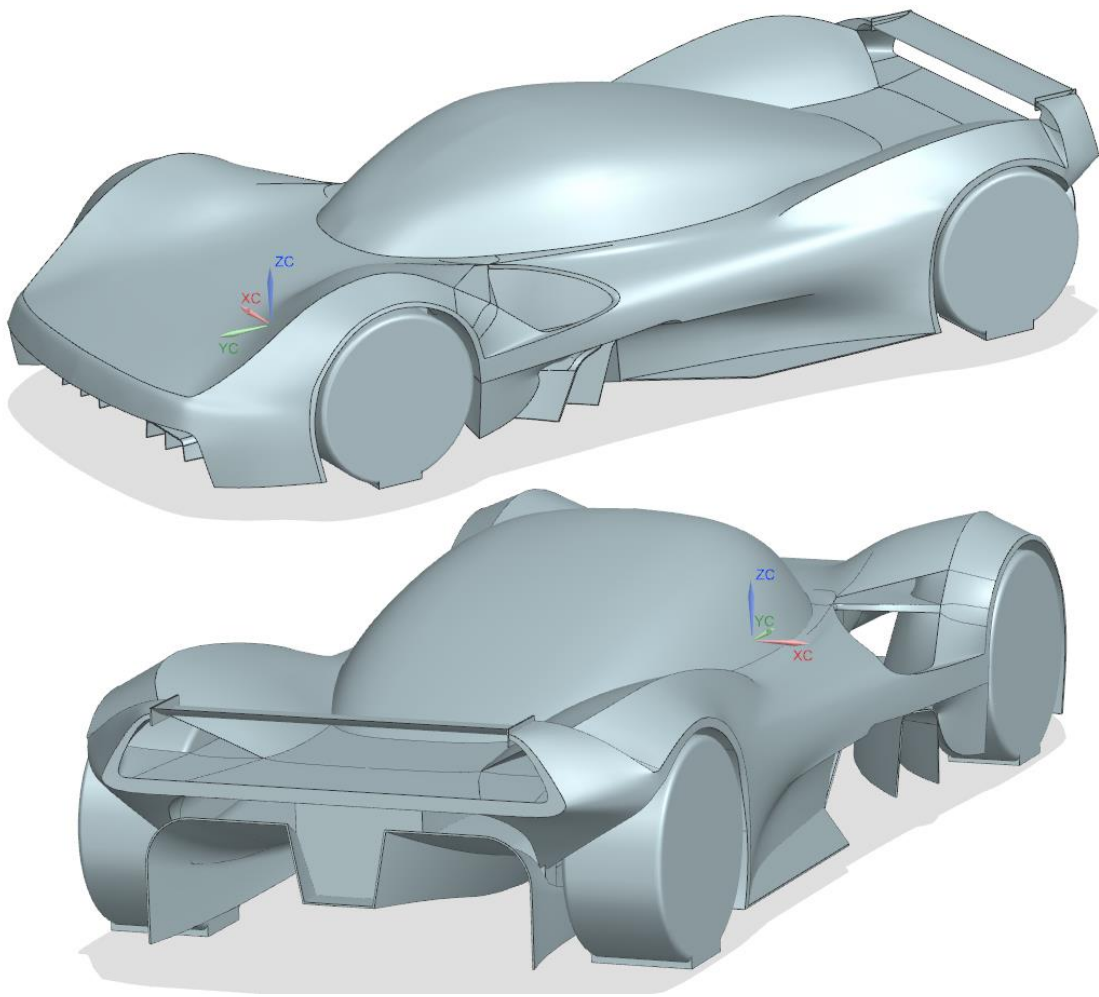


Figure 15: The final geometry with smooth edges hidden.

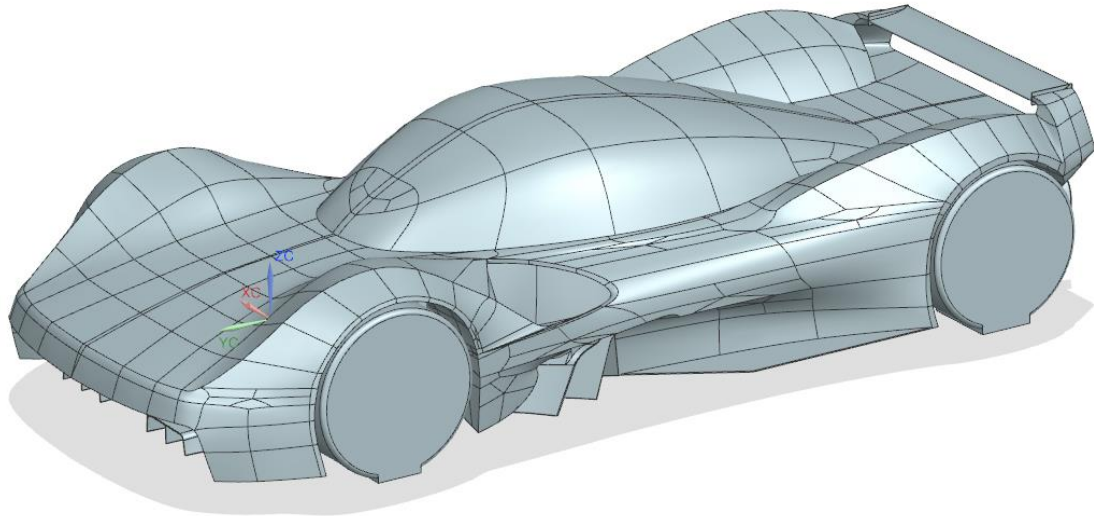


Figure 16: The final geometry with all edges shown. Having many edges and surfaces, some of which were small, caused multiple problems with mesh generation later in the process.

4.CFD setup

4.1. Mesh and boundary conditions

CFD analysis was done entirely in ANSYS software suite. Once the geometry was finished, it was halved across the symmetry plane, the computational domain was added and the car and wheels were subtracted from it. Meshing was performed in ANSYS Fluent Meshing module.

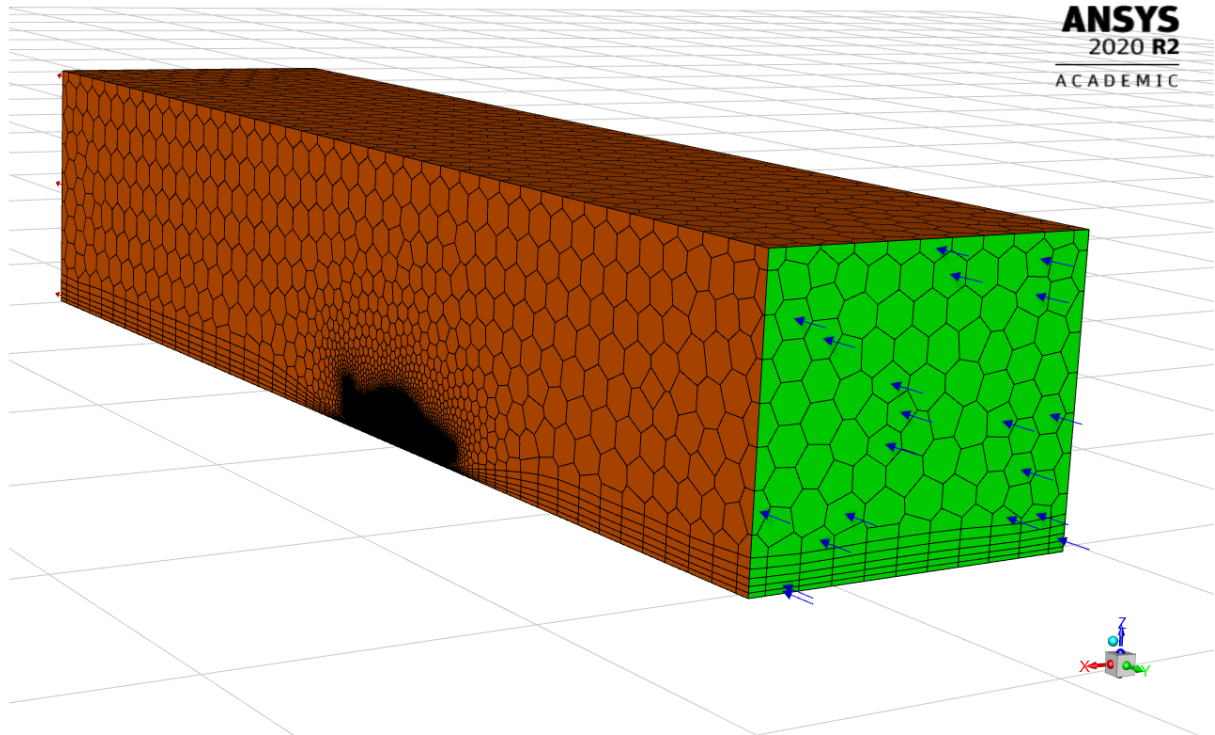


Figure 17: Mesh overview with visible cell edges and boundary conditions (symmetry in brown and velocity-inlet in green).

The computational domain is 29 m long, 7 m wide and is 5.8 m tall. Symmetry plane, roof and other side of the domain have symmetry boundary condition (shown in orange), velocity inlet has velocity of 50 m/s, turbulent intensity of 5% and turbulent length scale of 1 m. The floor is moving at 50 m/s, and wheels are rotating walls at 145.349 rad/s.

The mesh surface cells on the body and wheels have maximum size of 1 cm except the rear wing, where 1 mm mesh was used to properly model the airfoil's shape. Every wall was covered in 5-cell-thick boundary layer, including the ground, as seen on Figure 17, 18 and Figure 19. Its increased thickness there is not a problem though, because the ground is moving at the same speed as the free stream. The volume cells have tetrahedral shape, and a maximum size of 0.5 m.

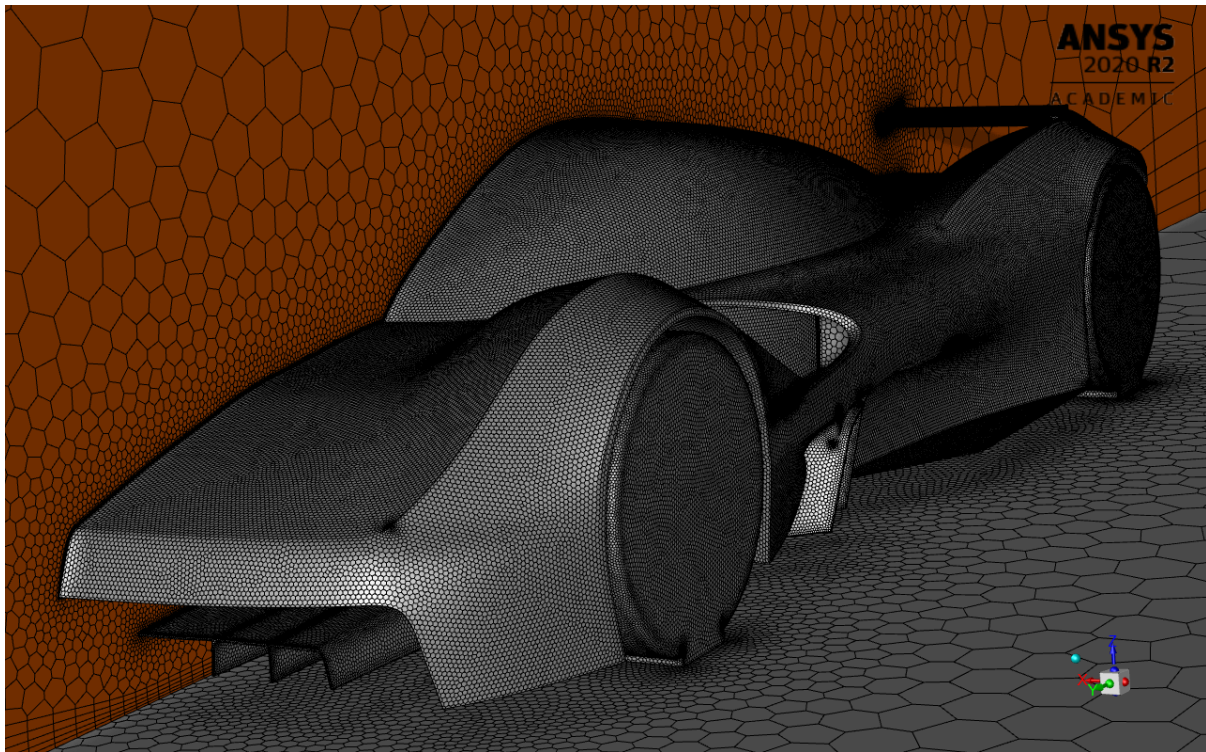


Figure 18: Detailed picture of the surface mesh on car's body and wheels.

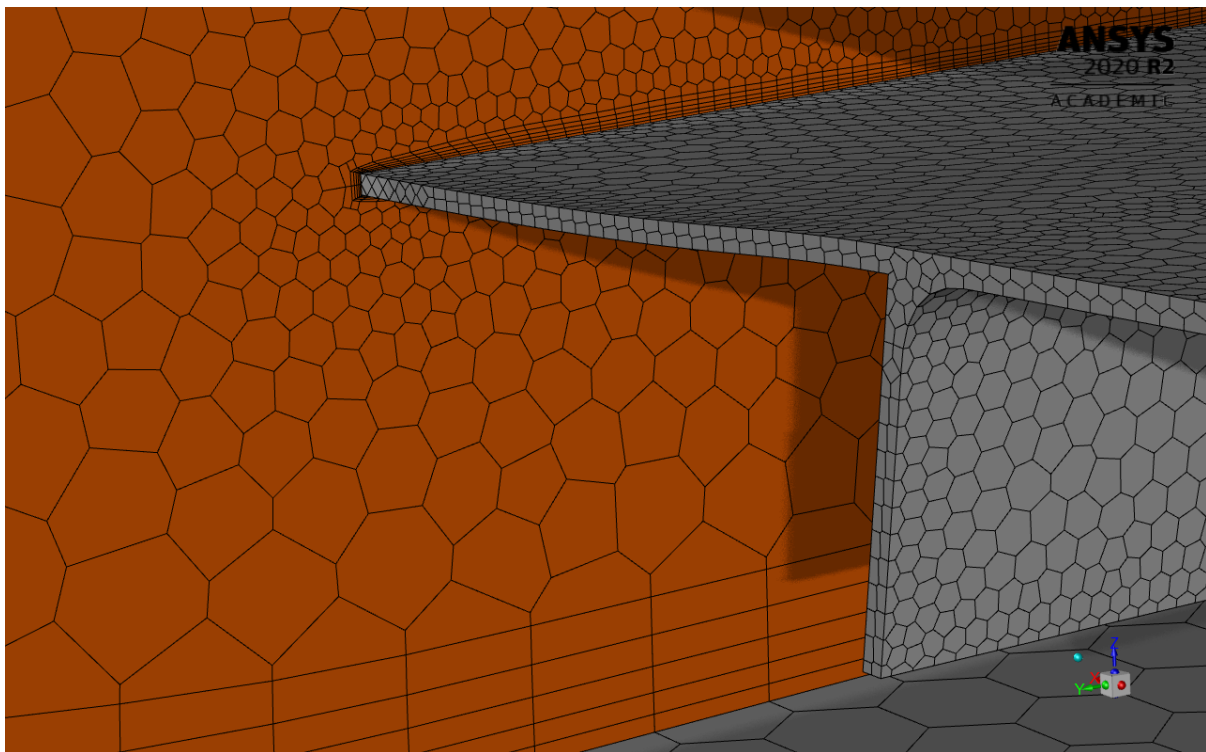


Figure 19: A close-up image showing boundary layer mesh on both floor and front tunnels. It should be noted that all thin surfaces used in the model have thickness set to 5 mm.

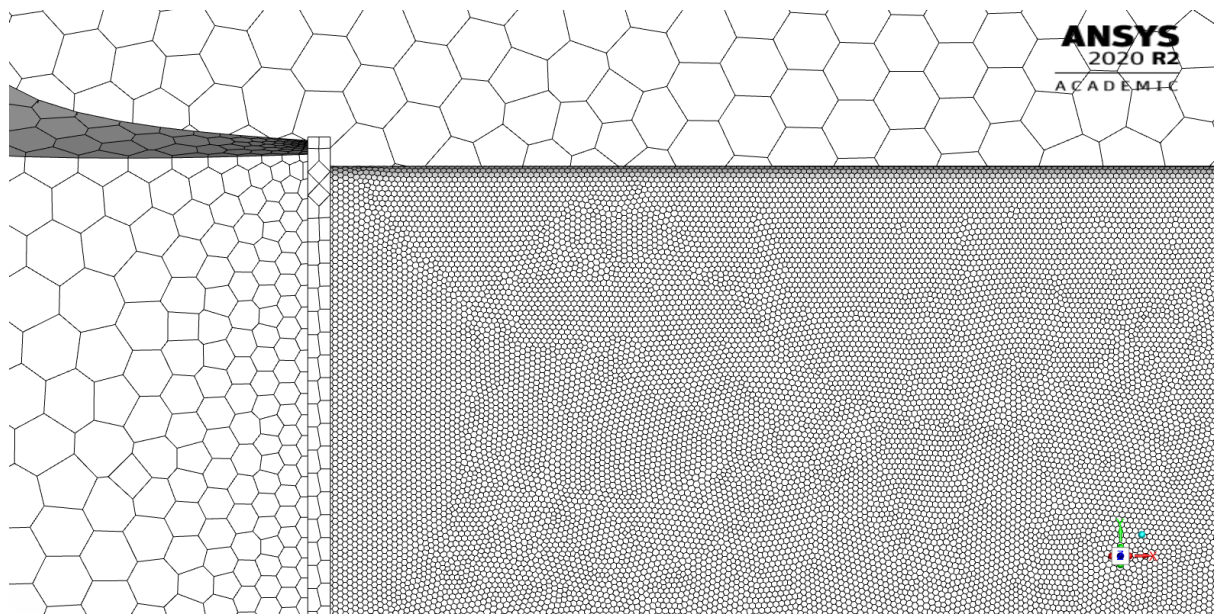


Figure 20: A close-up image showing denser mesh on the car's rear wing.

4.2. Models, methods and solver setup

Single-equation Spalart-Allmaras turbulence model was used with default parameters, as it is a standard approach for similar simulations at a similar complexity level. For heat exchanger, energy equation solution was added. The solver used was SIMPLE with the following spatial discretization settings:

- Gradient: Least Squares Cell Based
- Pressure: Second Order
- Momentum: Second Order Upwind
- Modified Turbulent Viscosity: First Order Upwind
- Energy: Second Order Upwind

5.CFD results

5.1. Convergence, quantitative results and validation

The results were achieved after a total of 668 iterations. To increase convergence speed, the solution was initially obtained with first order discretization, and then continued with second order discretization. Numeric values of the lift and drag are respectively -0.83 and 0.569 which gives a -1.46 lift-to-drag ratio - a disappointing number, considering the effort and influence of aerodynamics on the design of the entire car. An important step of results validation is performing a mesh density sensitivity analysis. While results of the drag coefficient seem convergent, lift coefficient does not seem to converge. This is probably either due to lower quality of 4 cm mesh result, or 1 cm with 1 mm on the wing being still too coarse to converge.

CL, CD vs. Surface cell size [cm]

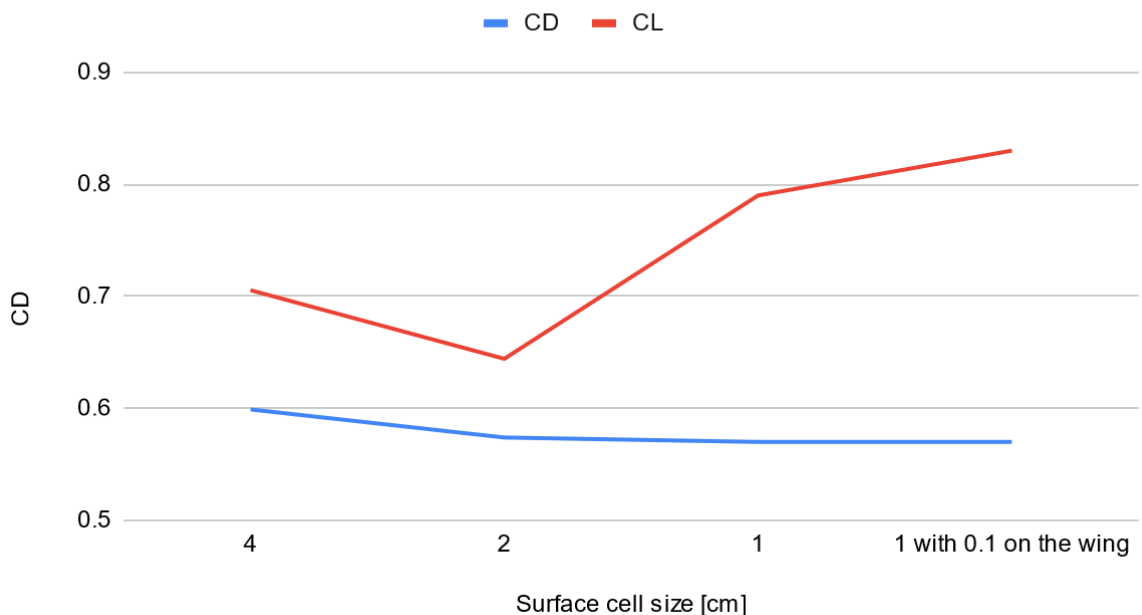


Figure 21: Values of CL and CD depending on the surface mesh density. For plot clarity, the sign of CL was flipped. The car produces negative lift.

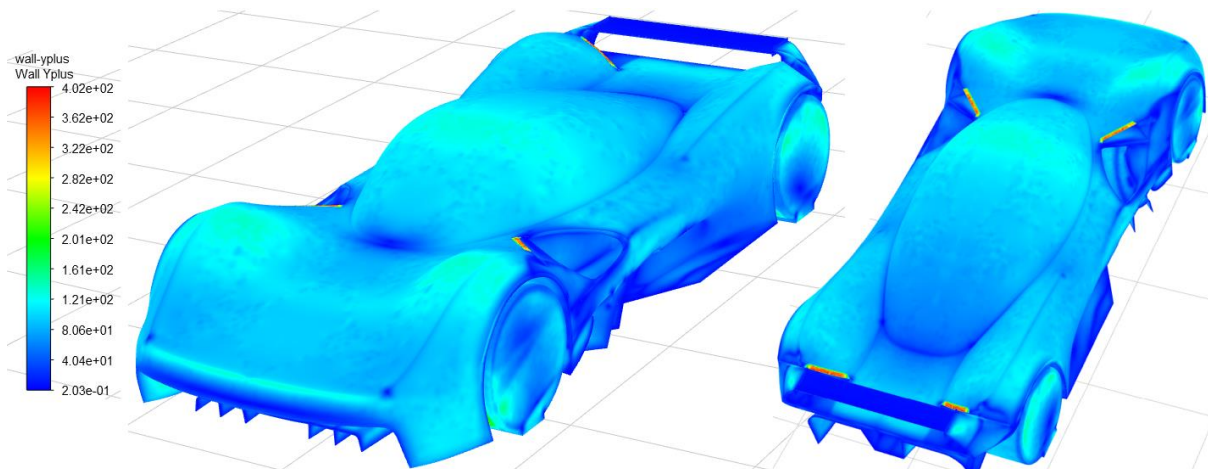


Figure 22: Values of $y+$ over the car's body and wheels.

The other element of validation was measurement of $y+$ values over the car's body. $y+$ only reaches unacceptably high values in two places, where there is a sharp edge with a very small angle between relatively large surfaces (Figure 22). This probably doesn't happen on the trailing edge of the rear wing because of a denser mesh there. A surface mesh with 1 mm max. cell size over the entire body would probably drive both extreme values mentioned before and the rest of the body into sub-50 range.

5.2. Initial pressure plots analysis

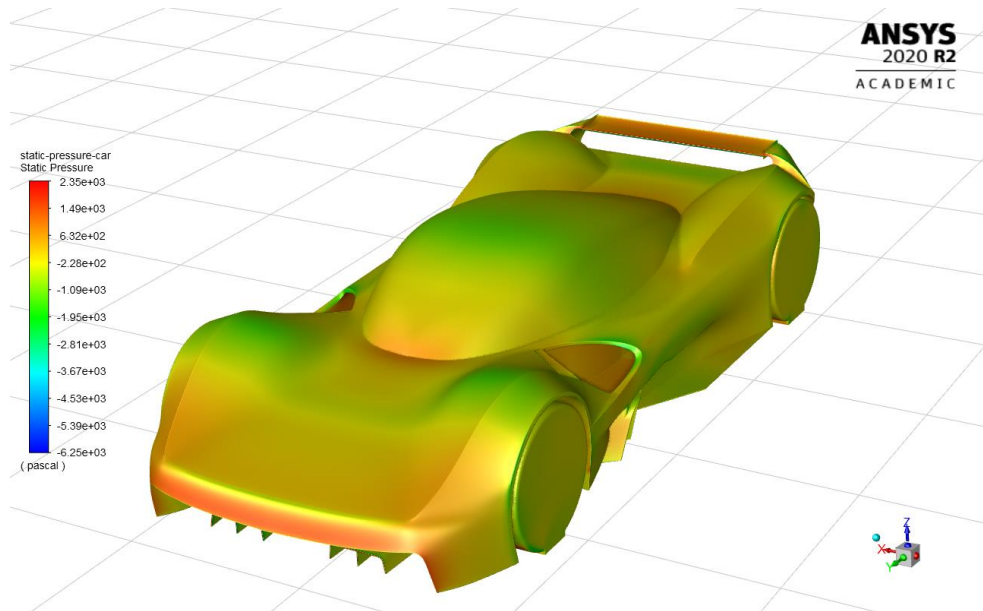


Figure 23: Significant pressure buildup on the front face, and a smaller one on the cockpit canopy. Large areas of negative pressure over the fender and the roof should also be seen.

From the Figure 23 it can be seen that the front face of the car generates a large area of high pressure, as well as significant separation at the leading edge of the body. The increased pressure on the windshield, internal tunnels and the rear wing is as expected. The other problematic part is having large areas of negative pressure on the front fenders, and especially on the roof canopy.

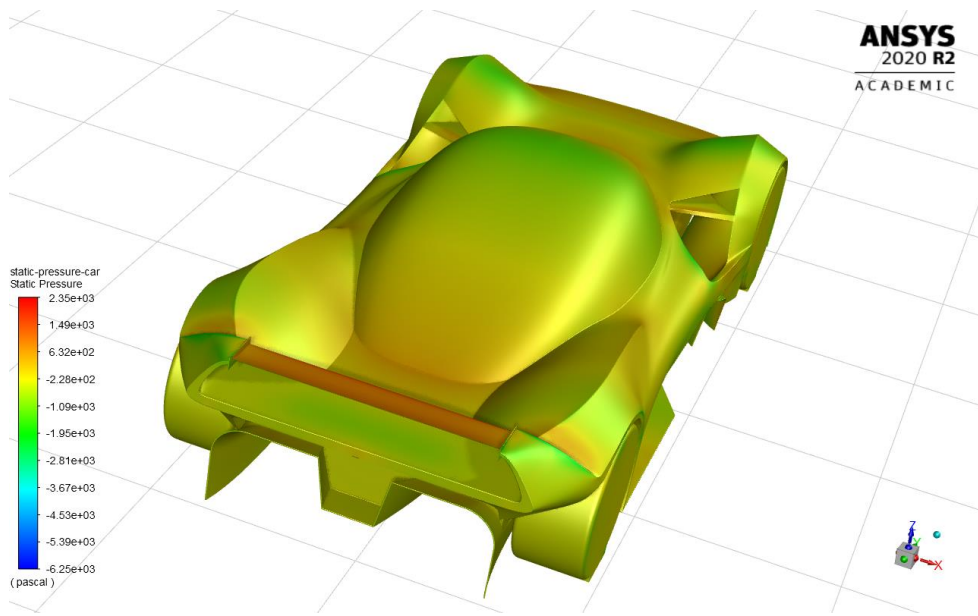


Figure 24: A smaller pressure buildup on the end of the cockpit canopy.

Figure 24 shows undesirable behavior at the end of the roof canopy. Having a smooth transition with the body would probably have decreased the pressure increase significantly and would probably have smoothed the flow leading to the rear wing. The shape of the integrated wing mounts also creates an avoidable separation.

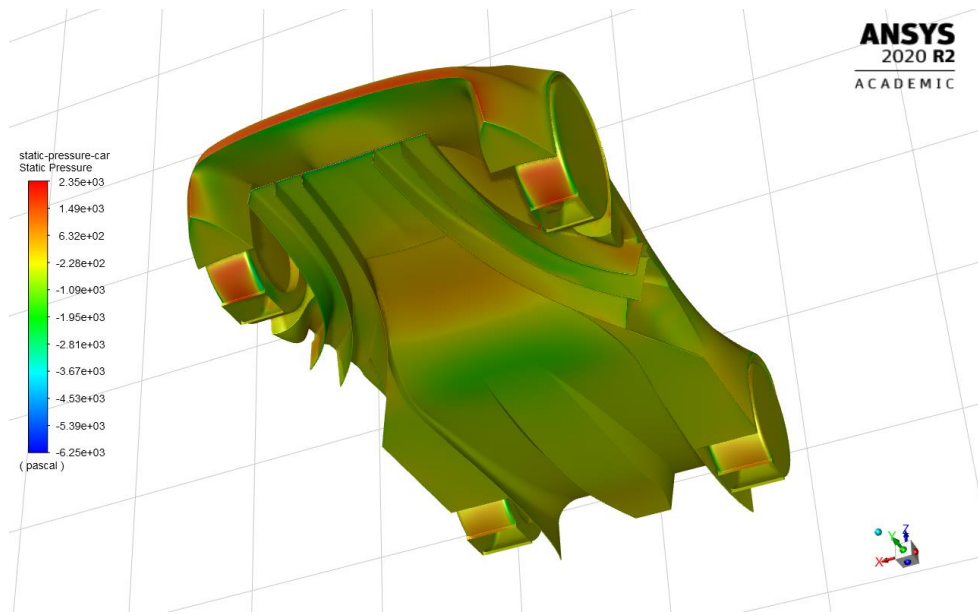


Figure 25: Large areas of negative pressure, combined with an area of positive pressure between them.

The contour plot on the Figure 25 uncovers that the separation on the front face of the car occurs also below its lower edge. This on one hand is a positive behavior, creating downforce at the most forward point of the car, but possible losses caused by introducing turbulence this early could negate the benefits. There is also a separation occurring at the leading edge of the front tunnels and the surface connecting them. This is caused by arbitrarily set thickness of all thin surfaces. The other problem is that while the center surface is producing downforce, it also leads the flow upwards, where it has no room to escape, having to collide with the tub, creating in turn a large spot of positive pressure. Right behind the positive pressure spot in the center of the underbody is the largest negative pressure area of the car. It is definitely in the desirable

place, but its size and numeric values are not sufficient. The last thing to note from this plot is that the channels of the front tunnels work differently depending on their position relative to the dividing surface. Only the outer channel seems to create any significant negative pressure, which due to the vicinity of the front wheel is not guaranteed to translate into useful downforce.

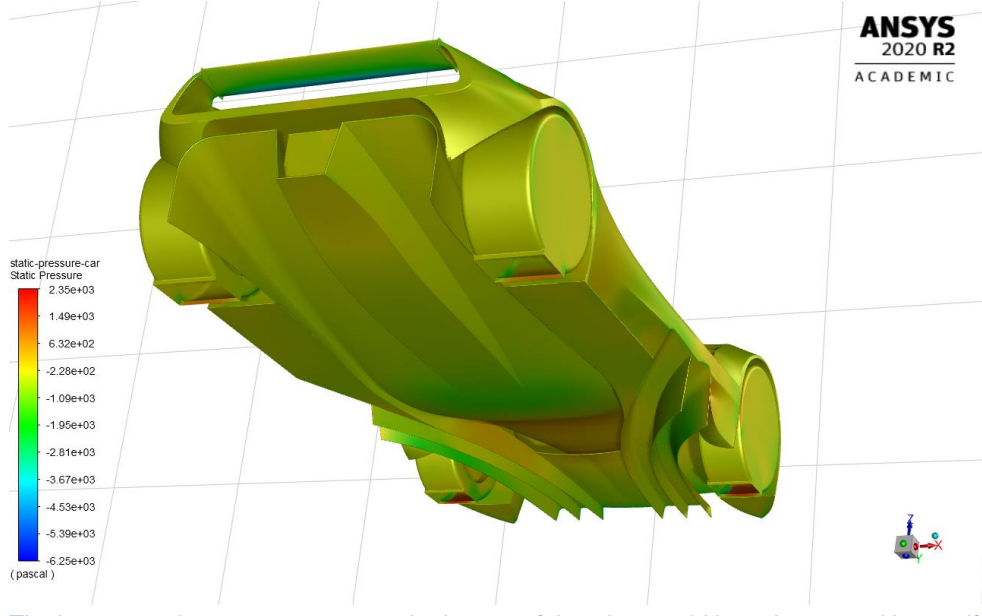


Figure 26: The large negative pressure area on the bottom of the wing would have been used better, if the wing were placed beyond the engine cover.

The rear bottom view only shows that the static pressure briefly grows near the end of the tunnels. The pressure buildup is accented even more, suggesting a need for even a small outlet.

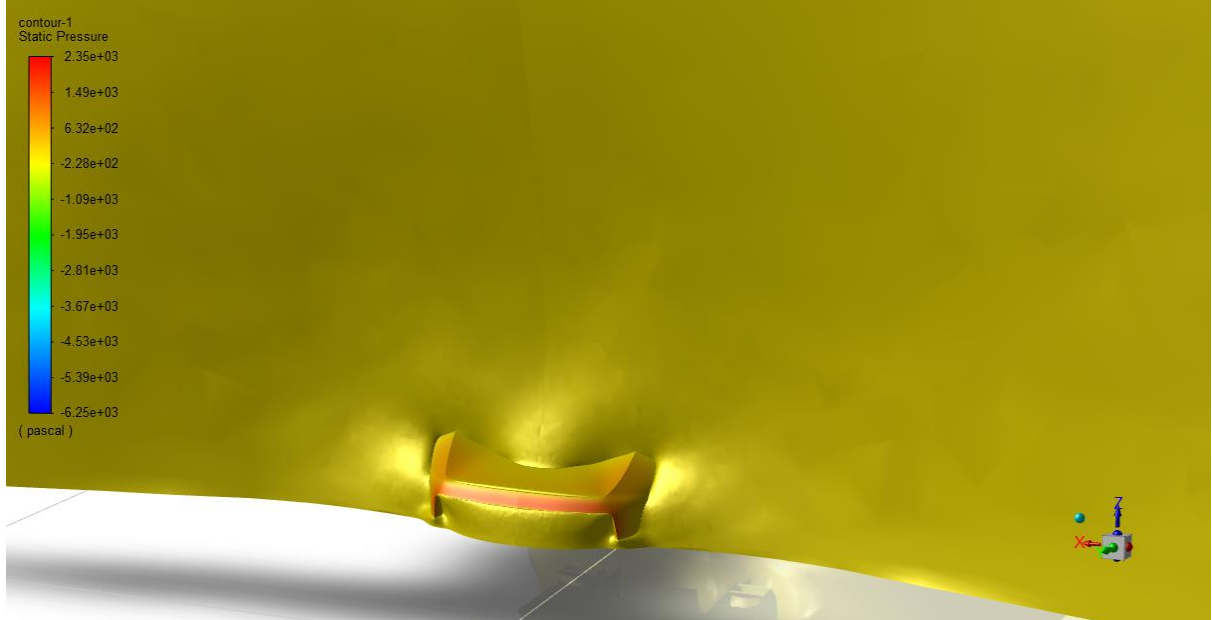


Figure 27: Surface of static pressure equal to zero indicating a bubble of high pressure being generated on the car's nose.

The following plots show the “bubbles” showing the surface of zero static pressure. This means that there is a large bubble of positive pressure building up in front of the car. This is not anything unexpected. Much more interesting conclusions can be drawn from Figure 28 – there is a positive pressure bubble created by the side radiator, which is just behind the front wheel

well outlet. This could possibly prevent it from working. Figure 29 shows several smaller high pressure bubbles spread around the back of the car.

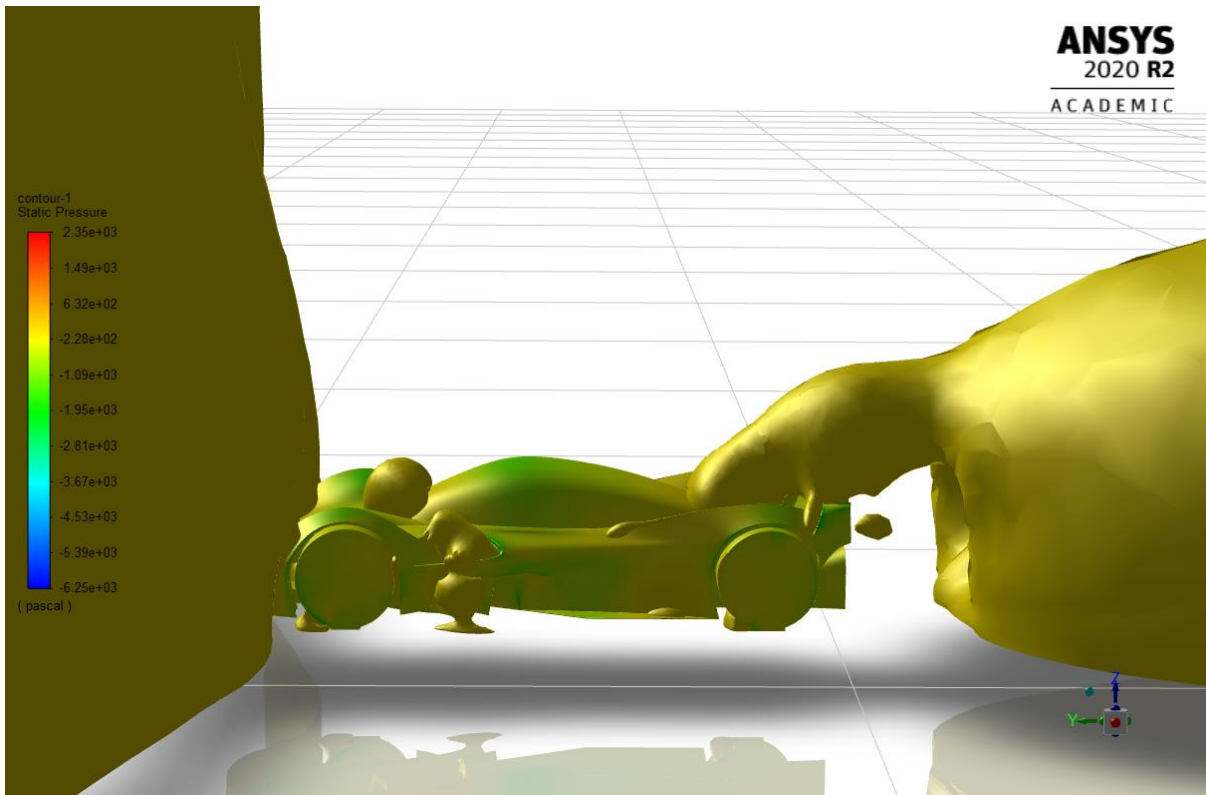


Figure 28: More pressure bubbles are forming on a windshield, side outlets and around the rear wing.

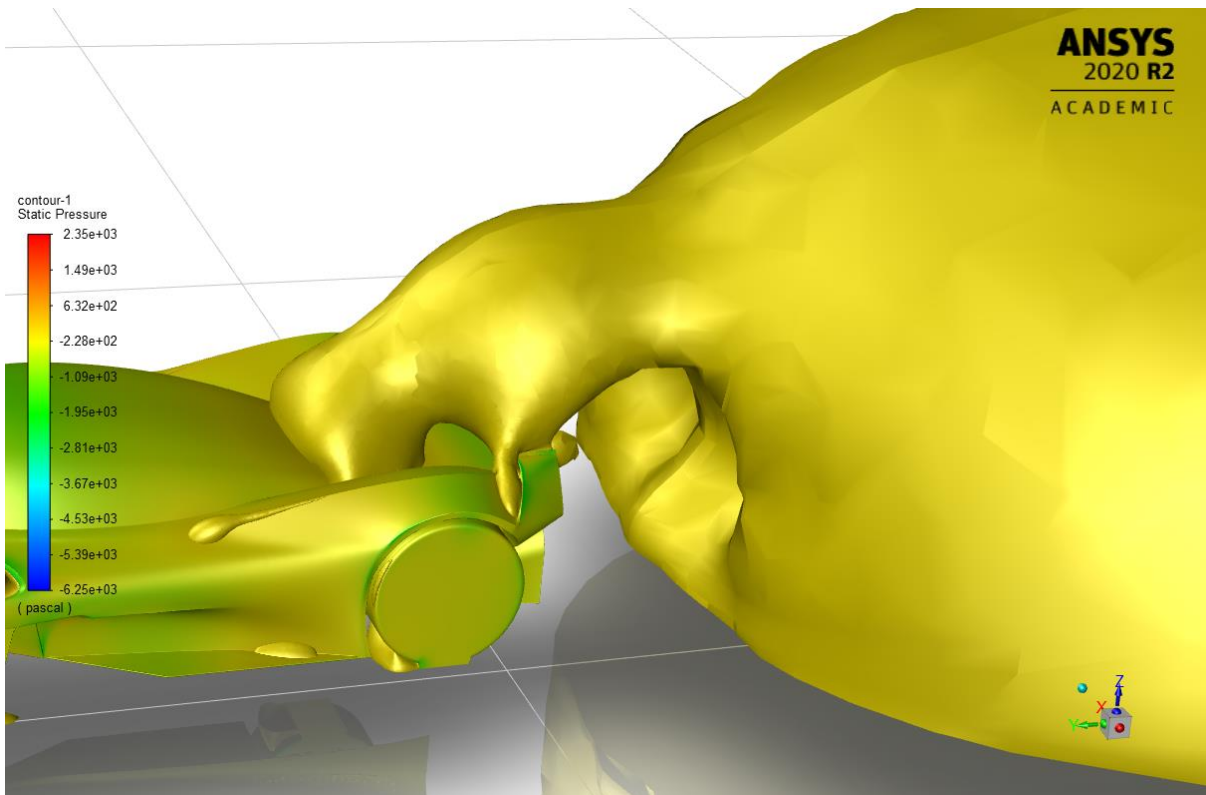


Figure 29: A small teardrop-shaped buildup of pressure in front of the rear fender is caused by the fault in the mesh (end of a sharp edge).

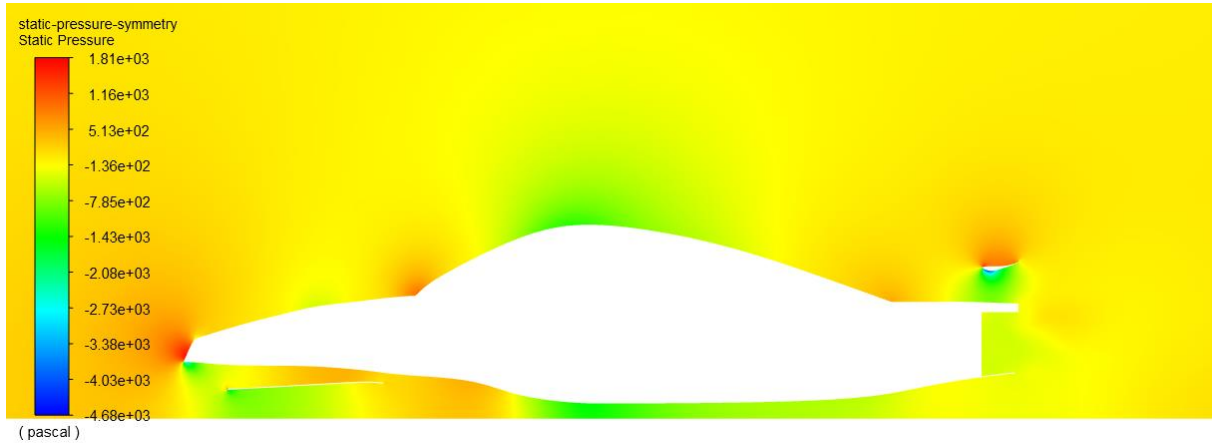


Figure 30: qualitative plot of pressures around the car's body.

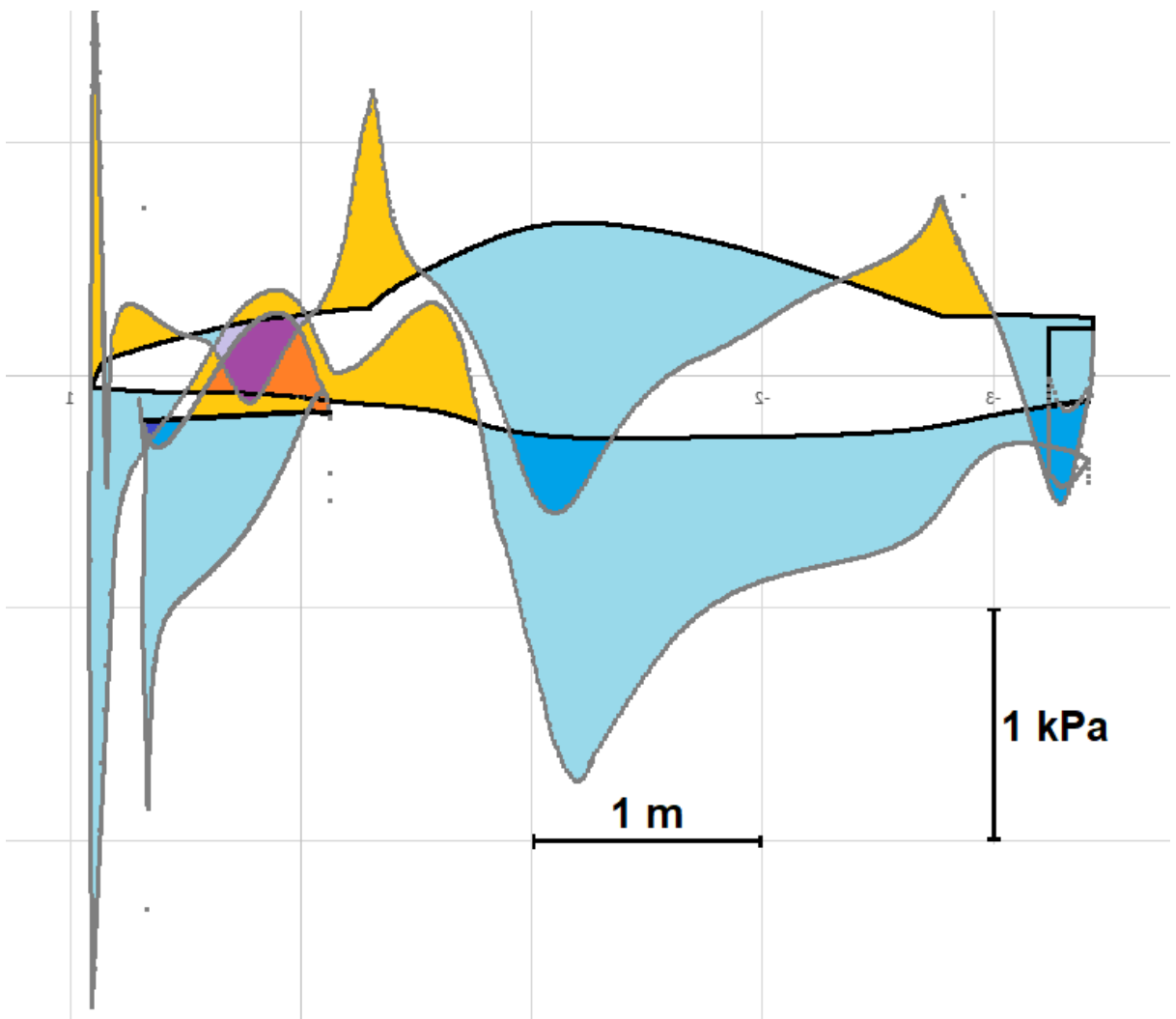


Figure 31: XY plot with scaled pressure values added over the car's surface. Blue areas represent negative pressure and orange represent positive. The shades only help visualize overlay of those areas.

The line plot (Figure 31) confirms the previous observations - while there is negative static pressure on the bottom surface of the car, there is also a lot of the negative pressure in the upper surface, and the difference is insufficient to create the desired lift coefficient.

5.3. Detailed flow analysis

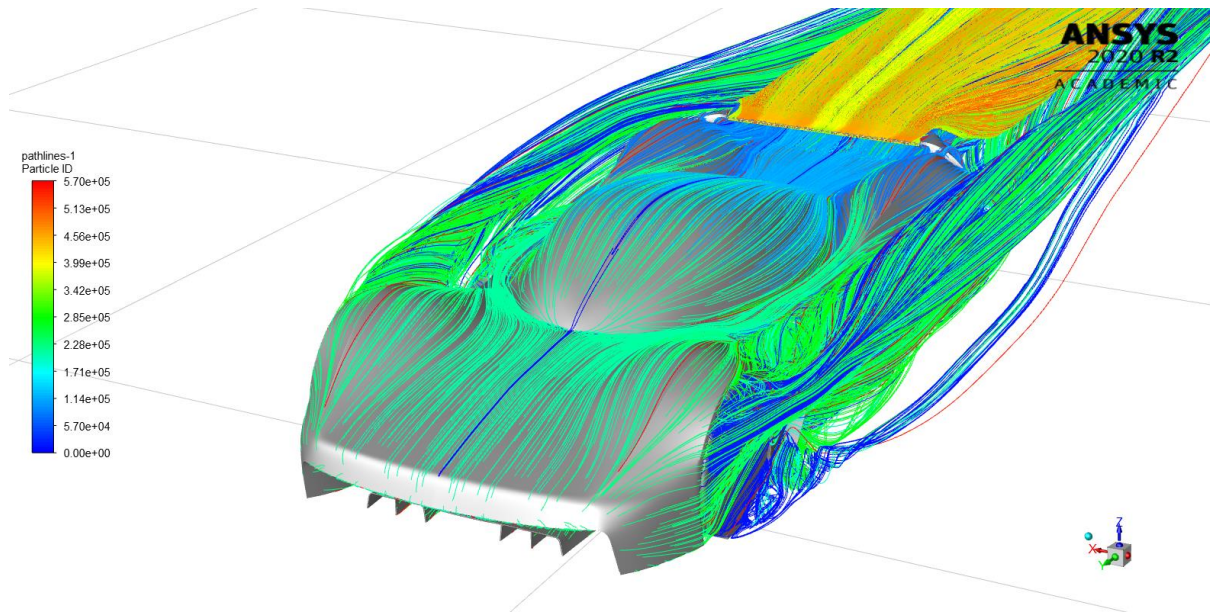


Figure 32: Major vortices shed from the top of the front wheels and minor from the bottom.

The basic view of the flow (Figure 32) indicates the existence of two major vortices being generated by each of the front wheels. The top one is connected to the top fender, and sheds without further influence on the car's airflow, while the bottom one sticks to the ground and also continues undisturbed. This is confirmed by separating the flow starting from the front wheels (Figure 33).

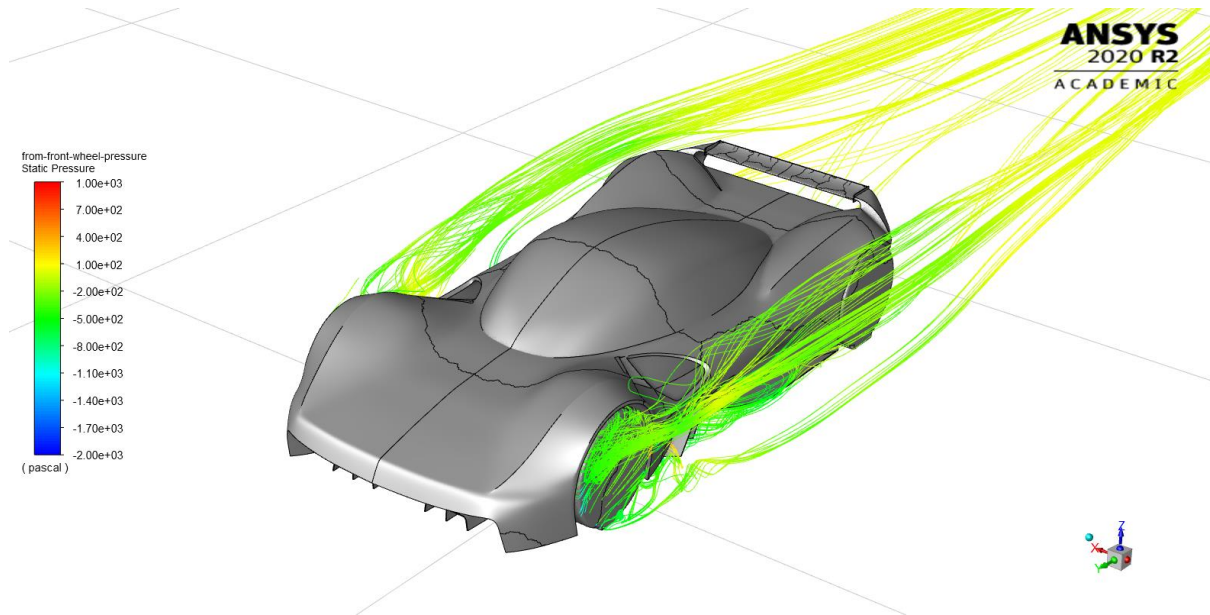


Figure 33: Limiting pathlines to only those starting from the front wheels confirms that the front wheels are responsible for two large vortices on each side of the car.

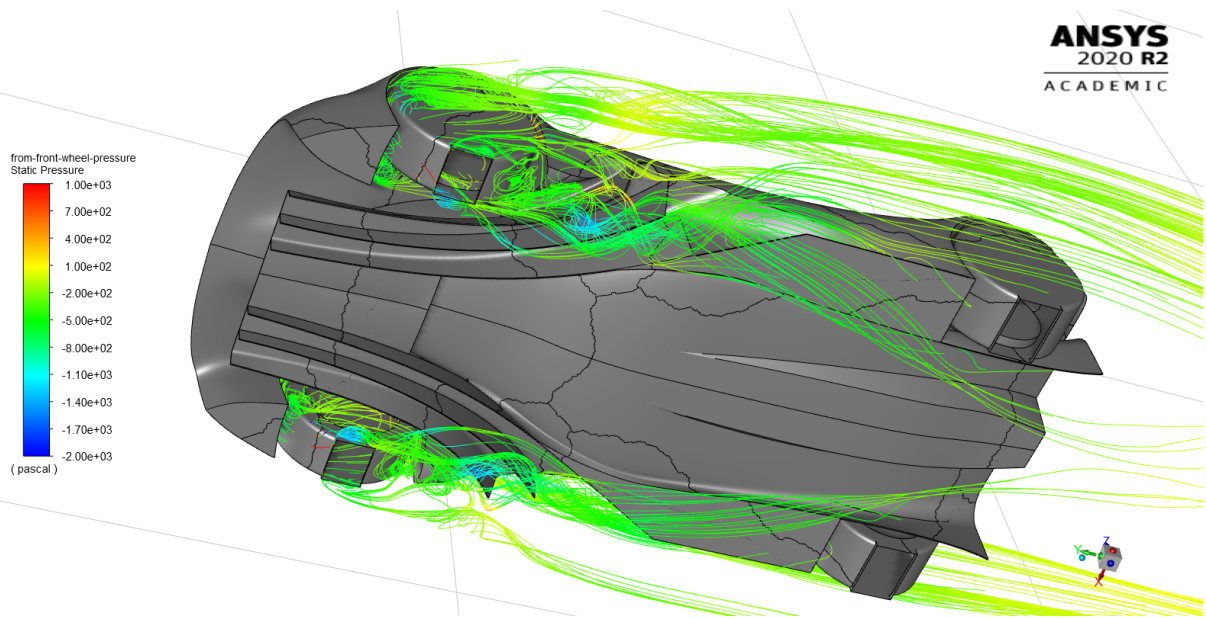


Figure 34: Front wheel wake seen from the bottom. It should be noted that the turbulent flow enters the front tunnels, and then later the rear tunnels as well.

Further analysis of the front wheel wake uncovers disturbed flow that enters the exit of the front tunnels and continues partially to the car's side, but a major part goes under the side floor extensions and enters the rear tunnels, possibly disturbing their flow (Figure 34). A possible solution to this problem could be sealing the rear part of the font tunnels from the bottom, as seen in all LMP1 cars (Figure 35).



Figure 35: Toyota TS050 front diffuser inlet and exit. [1], [3]

The overview of pathlines seen from the rear (Figure 36) indicates that the rear wheel pressure outlets are working correctly, but a closer look on the front ones shows a complex interaction between the top outlet, wheel wake and the large opening below. It's possible that the positive pressure exiting through the opening (Figure 28) diverts the flow exiting through the outlet and leads it into the vortex shed from the top of the front wheel (Figure 36), resulting in making it stronger.

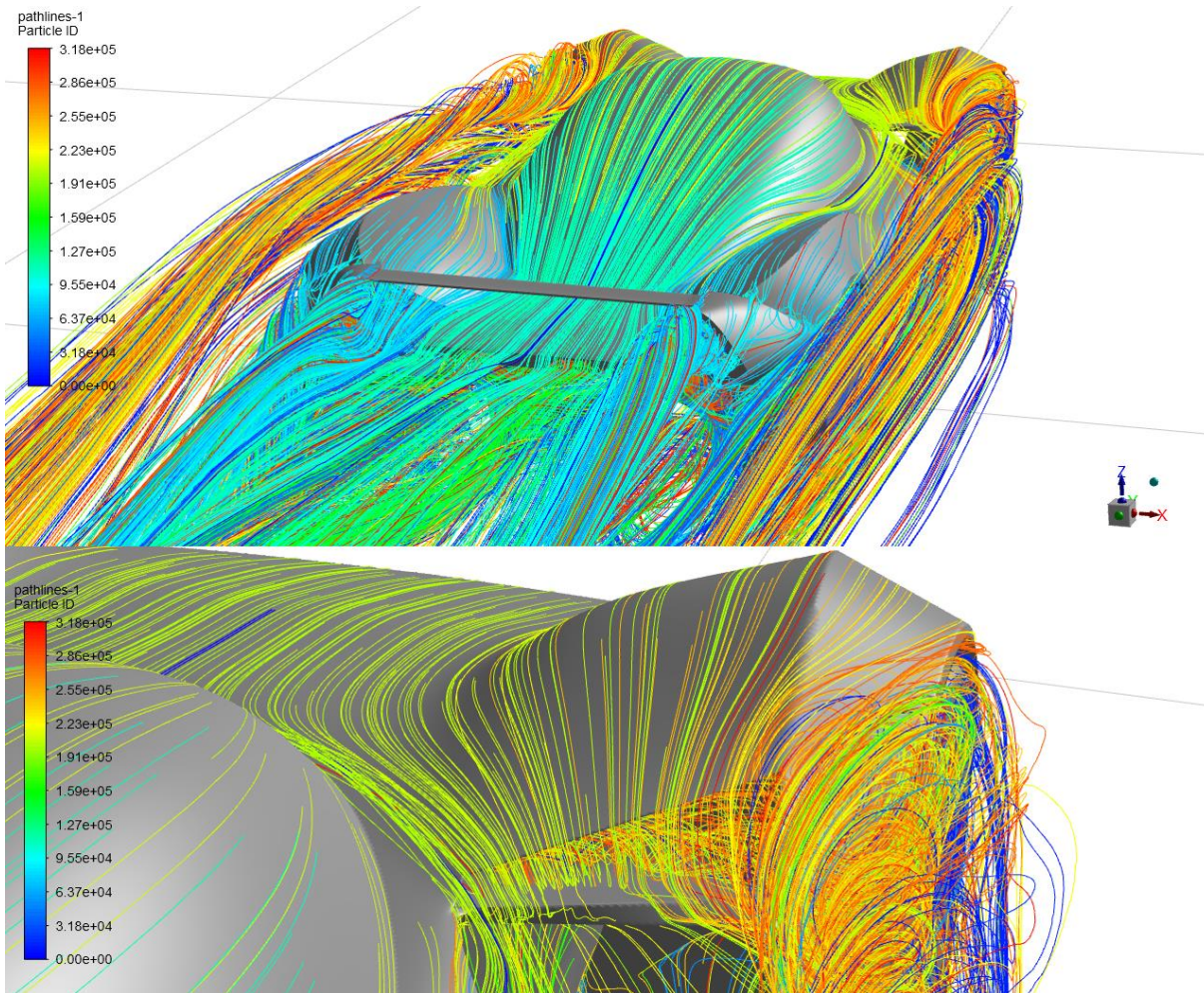


Figure 36: Constant-color pathlines seen from the back. While rear wheel outlets seem to be working properly (top), the front wheel outlets seem to be feeding the vortex shed from the top of the front wheels.

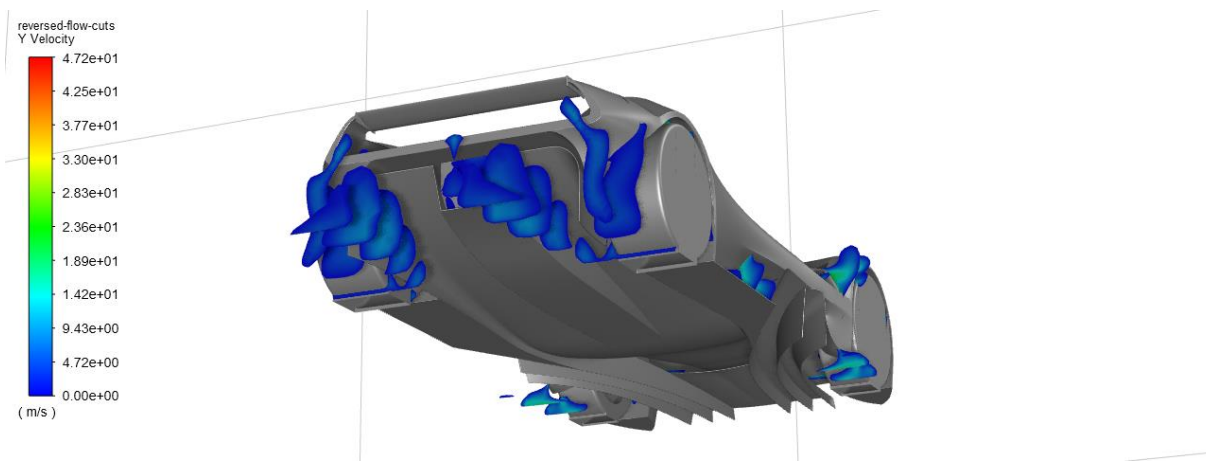


Figure 37: Plot of positive Y-velocity showing areas of reversed flow in vicinity of the rear tunnels.

Reversed flow analysis was performed by plotting contours of positive component of velocity in the car's driving direction (Figure 37). It can be seen that the reversed flow enters the tunnels in a considerable way almost up to the point of the rear axis. To track the exact flow, another plot of pathlines colored by Y-velocity was made (Figure 38).

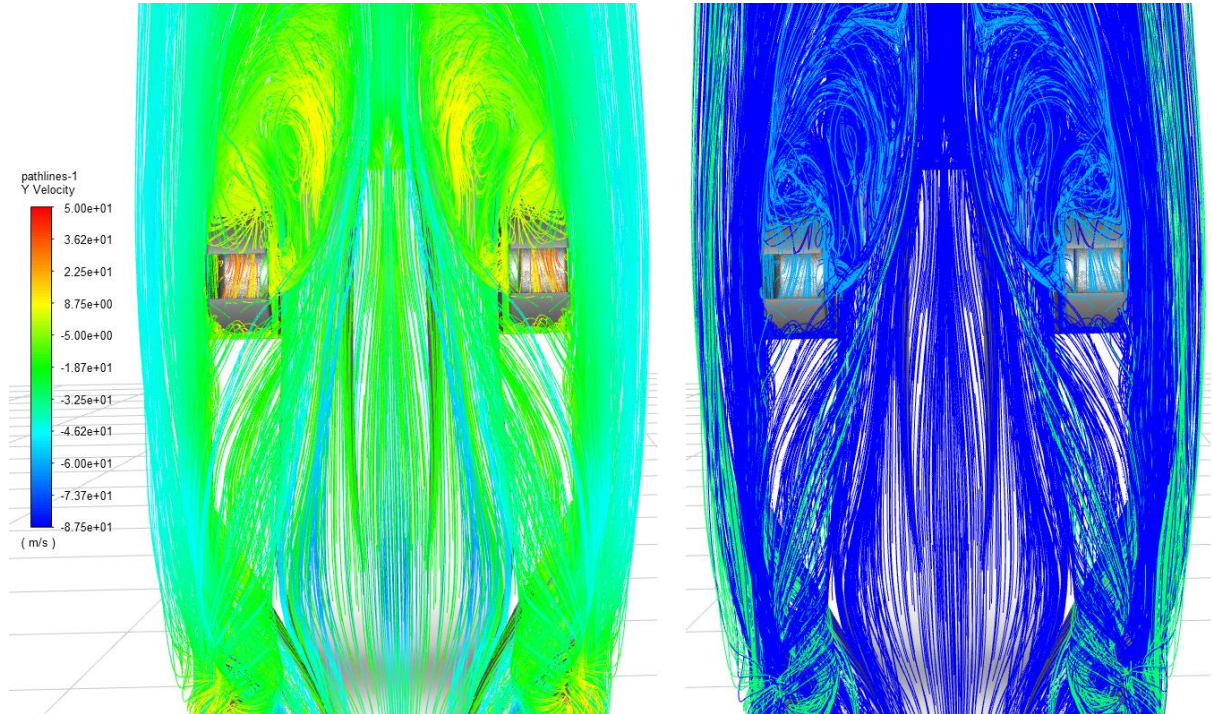


Figure 38: Closeup on the rear of the car, seen from the bottom. Pathlines colored by Y-velocity (left) and by their source surface's ID for comparison (right). Reversed flow is the area in yellow.

This is definitely an undesirable behavior. Probably the major cause of this is not having enough low pressure and high velocity flow in the tunnels. Possible minor solutions to this problem would be lowering the ground clearance, extending the diffuser vertical side and installing additional aerodynamic devices on the bottom edge of the diffuser (Figure 39).

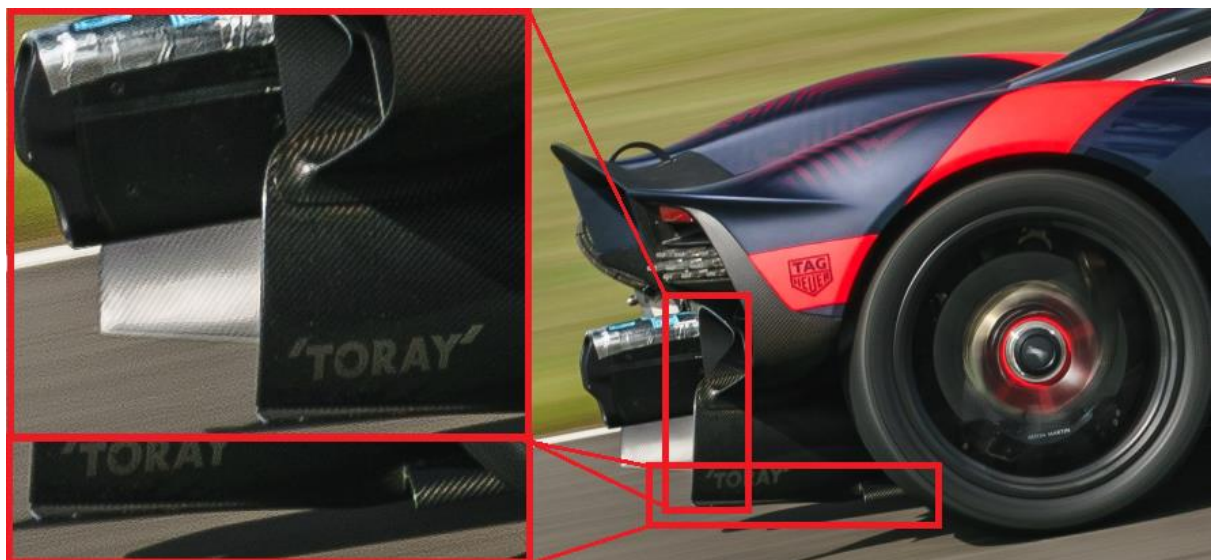


Figure 39: Aston Martin Valkyrie rear diffuser exit with detailed side extensions and bottom edge. [2]

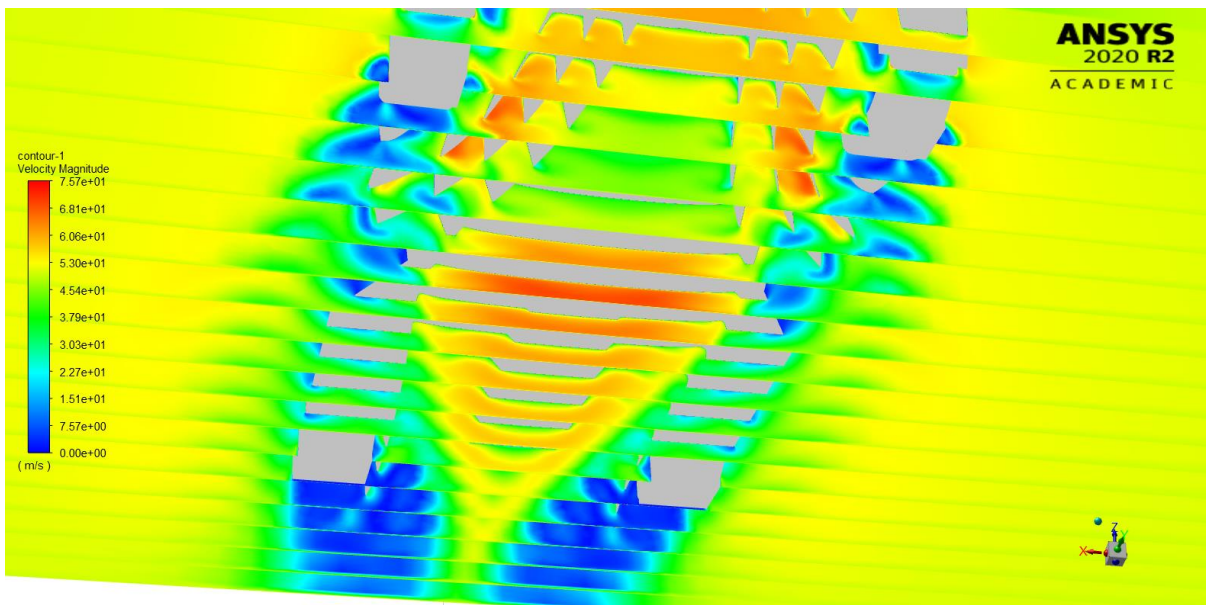


Figure 40: Velocities are as expected knowing pressure distributions, but the flow in the rear tunnels suggests problems with vortex generation.

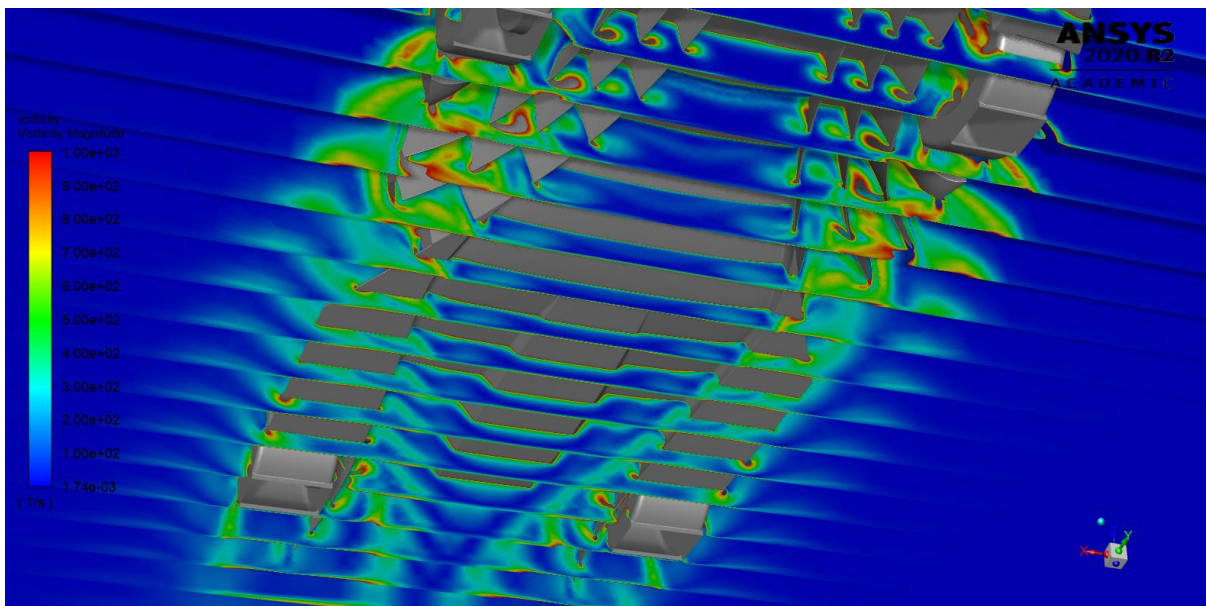


Figure 41: Vorticity contours on several planes. Note: Vorticity plots are symmetrical due to the fact that only "half" of the flow was simulated.

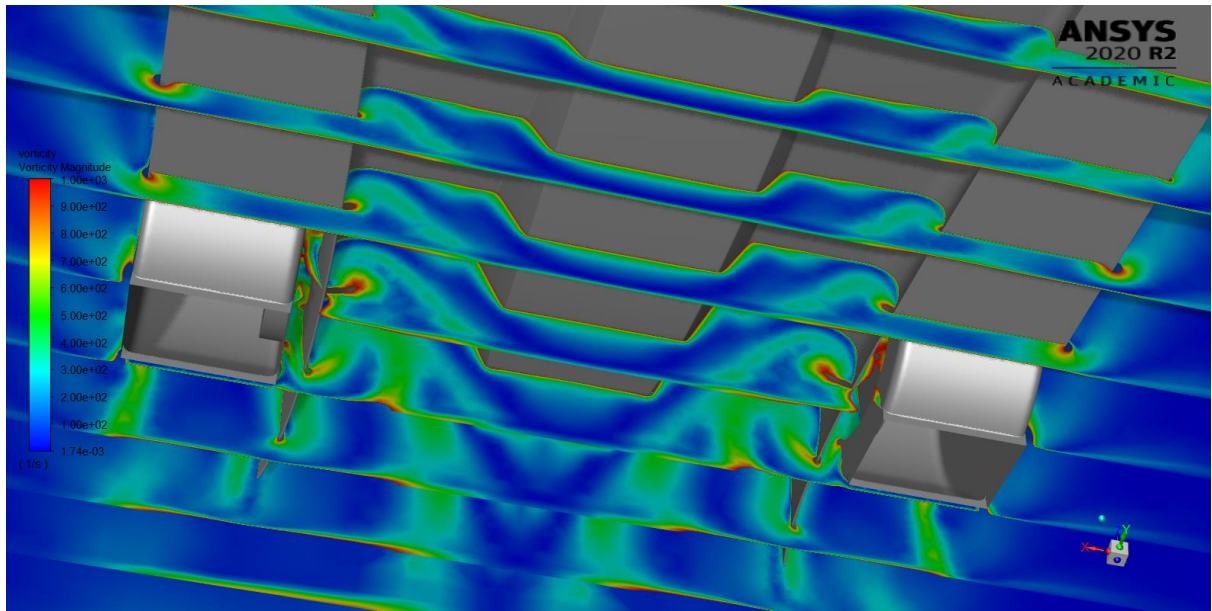


Figure 42: Vorticity in the rear tunnels starts only around the rear axis. Also, flow around the edge of the side floor extensions should be noted.

Vorticity analysis (Figure 41, Figure 42) preceded by velocity plot (Figure 40) shows expected differences in vorticity in front tunnels partially caused by influx of the front wheel wake, but also shows surprising lack of vortices in the rear tunnels, with the vortices starting around the rear axis. Another interesting effect is the occurrence of small vortices at the edges of the footplates. This is often managed by using curved footplates (Figure 43).

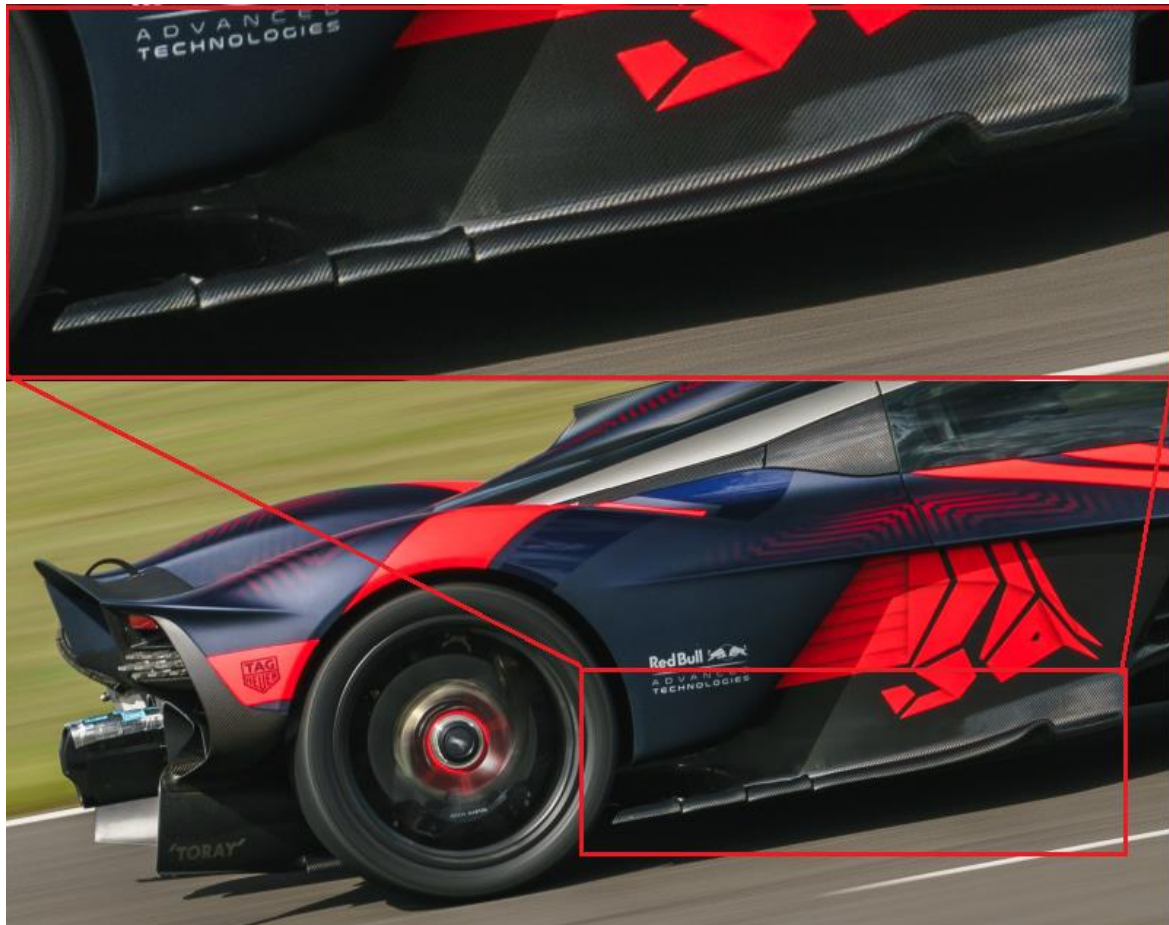


Figure 43: Aston Martin Valkyrie side floor extension footplates. [2]

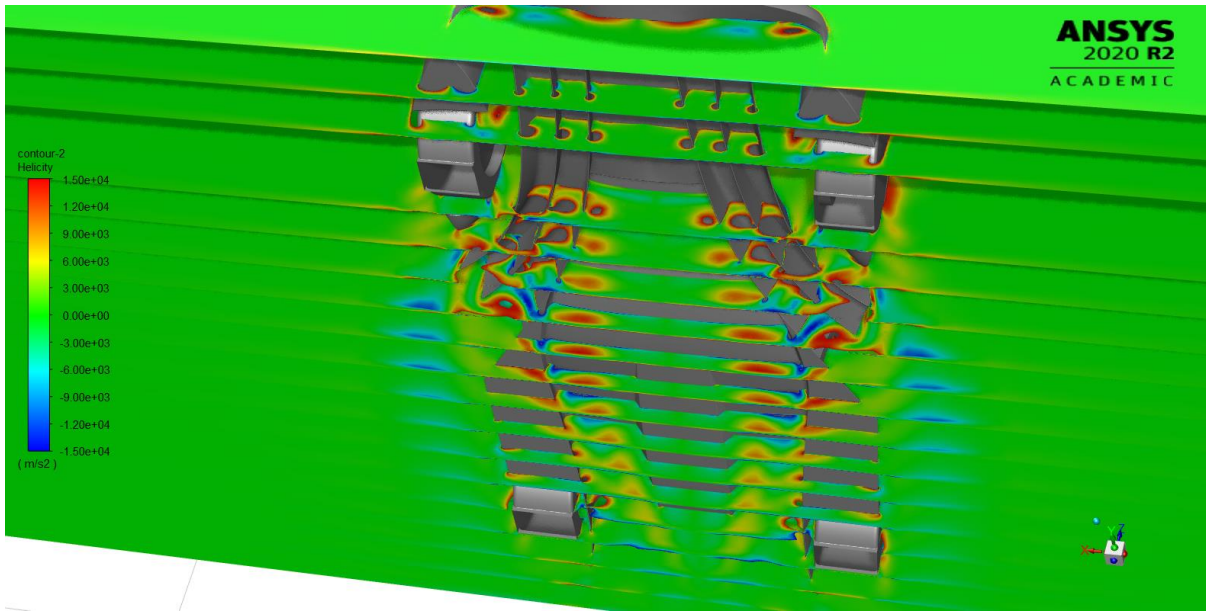


Figure 44: Helicity plot showing vortices progression down the flow. Note: like with the vorticity contours, only the left side of the car has correct values.

Helicity plot (Figure 44) shows the existence of vortices generated by the leading edges of vertical surfaces of the front tunnels. These vortices, if properly managed, could be a valuable source of downforce. The vortices generated inside the front tunnels seem to suffer from interaction with the front wheel wake, and the vortices that continue into the rear tunnels seem to weaken along the flow, probably due to the inflow of the air from below the side floor extensions. Another possible problem is ride height being too high, as the dependency between ride height and diffuser efficiency is mentioned in [8].

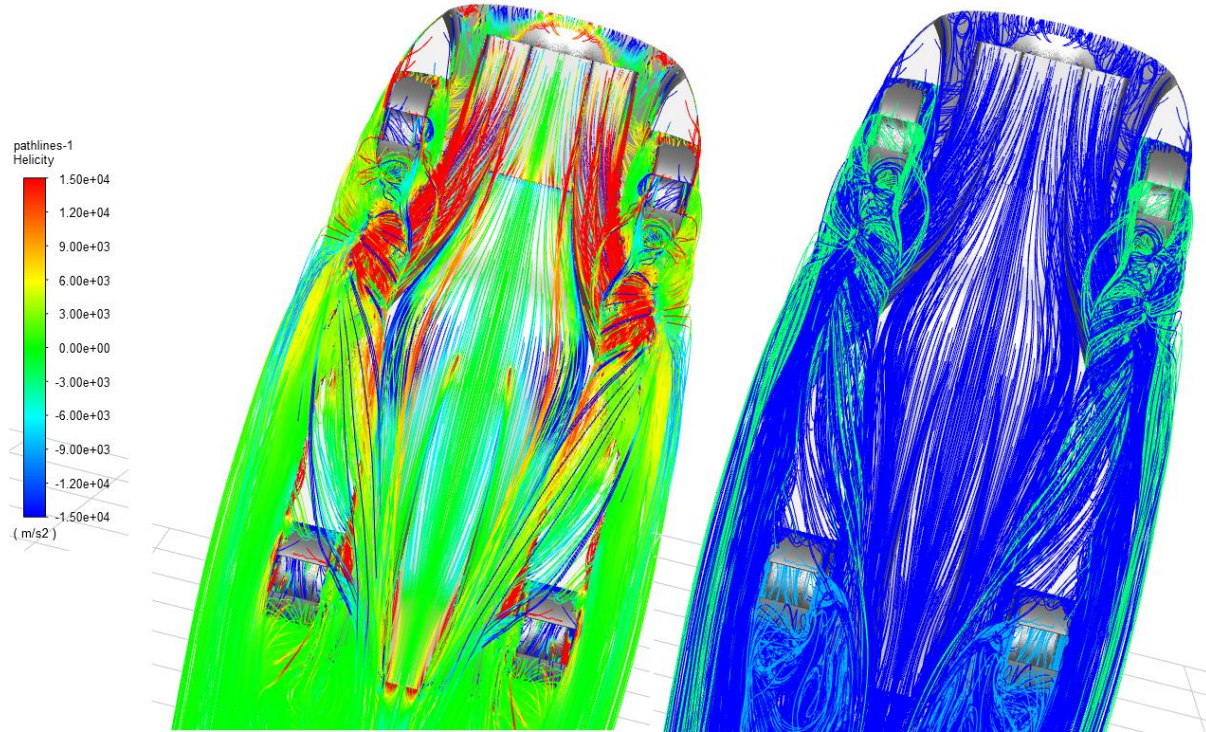


Figure 45: Helicity-colored pathlines (left) and source surface ID-colored pathlines for reference (right).

Helicity-colored pathlines (Figure 45) confirm these suspicions. Front wheel wake enters the front tunnels, wraps around the front tunnel vortices, exits the tunnels and later wraps around

the side floor extensions and enters the rear tunnels as well. To finally investigate the influence of these vortices a comparison with experimental results was done using oil flow visualization, which is considered to be closest to the real-world experiments. Both textbooks [4], [6] and experimental research, such as [10], links the downforce created by the diffuser with the vortices being created inside it. As multiple oil pattern experiments were performed, all of them included significant lateral flow caused by the vortices. For a comparison, oil flow plots were performed in the simulation, showing no lateral movement, suggesting lack of remarkable influence of the vortices inside.

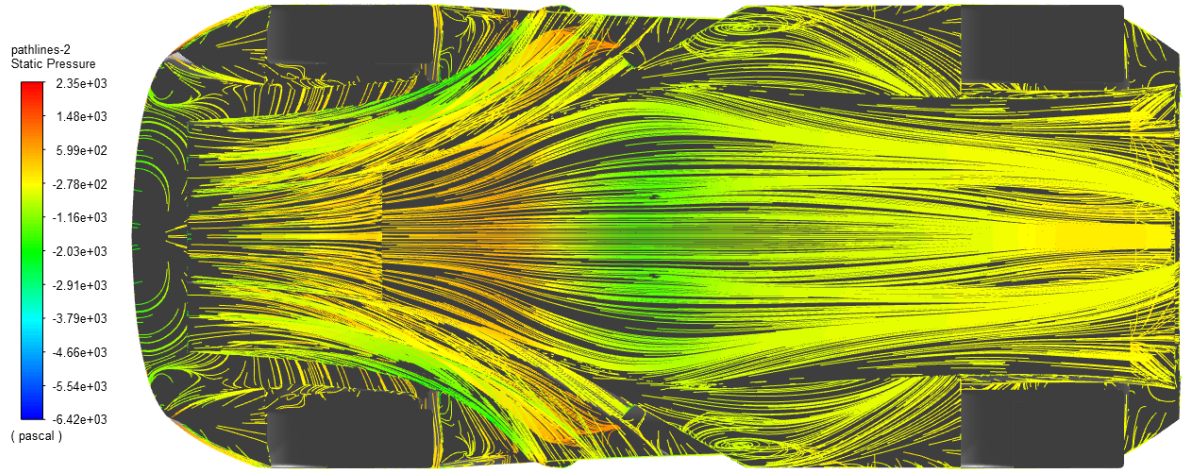


Figure 46: Oil flow visualization of the car's floor. No influence of vortices is visible on the surface of the rear tunnels.

Total pressure of the flow is reduced only by the moving car, so plotting total pressure losses could be used to determine areas of drag generation (Figure 47 and Figure 48). The main areas of heavily slowed down flow were front wheel upper vortices and rear wheel wake. Influence of other components of the front wheel wake is also noticeable, but it has smaller significance.

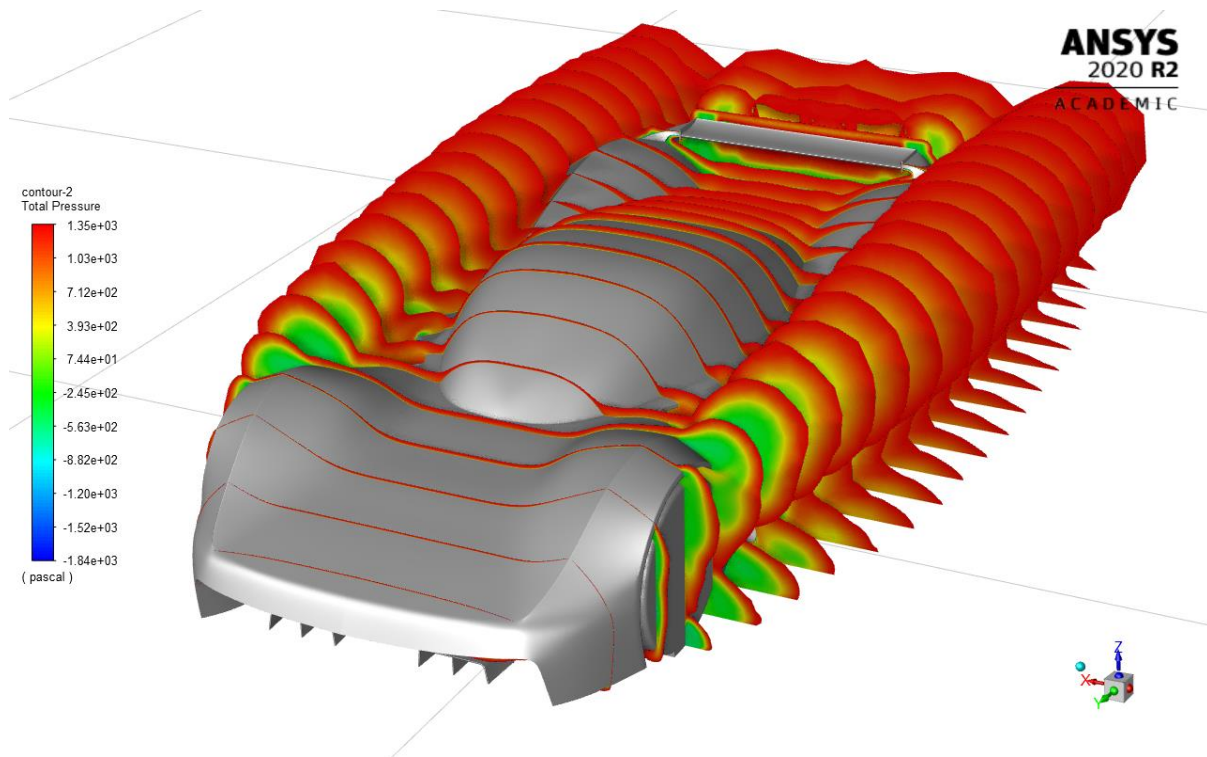


Figure 47: Total pressure losses. Front wheel wake seems to produce a lot of drag except reducing downforce.

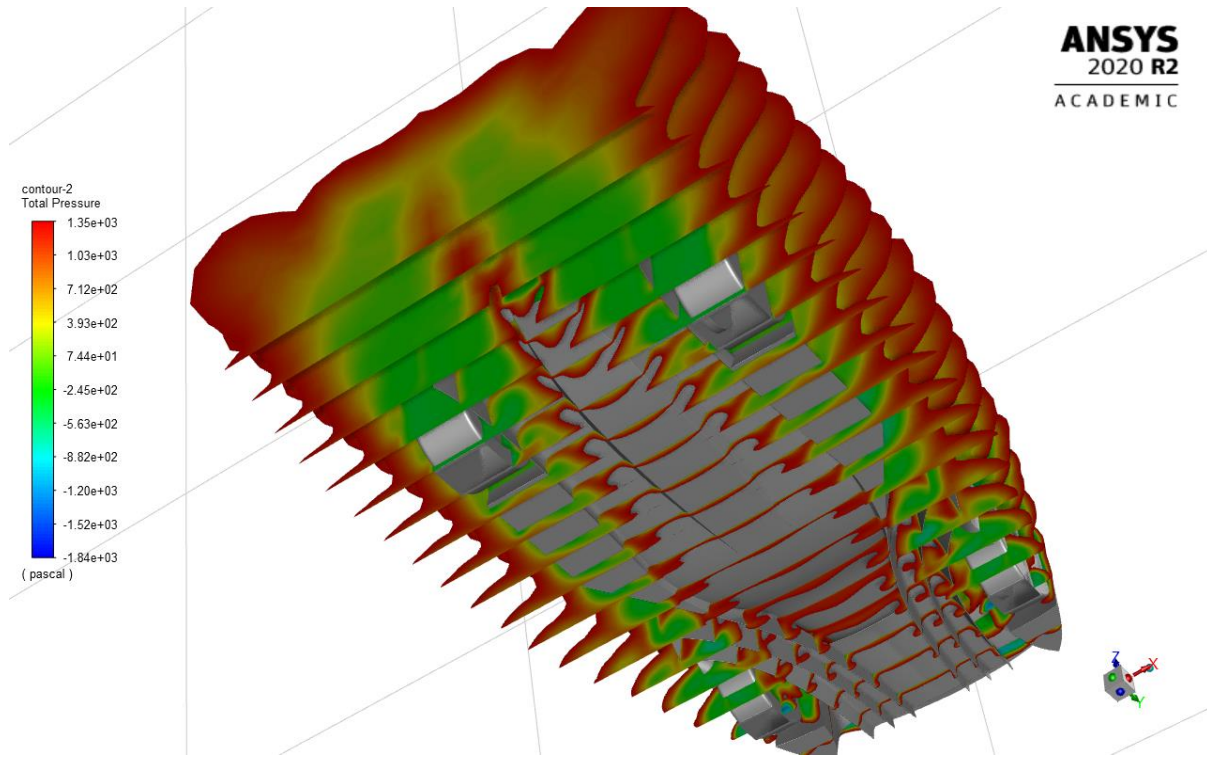


Figure 48: Total pressure losses in the back. The losses start appearing around the back just where the rear wheel wake enters the rear tunnels.

5.4. SAS transient analysis

To further and more accurately investigate behavior of the flow, a transient SAS (Scale-Adaptive Simulation) analysis was performed. Having a max. surface cell size of 1 mm on the rear wing and free stream at 50 m/s, time step of 2e-5 was used. To visualize the vortices, iso-

surfaces of Normalized Q-criterion = 0.1 were created. Q-criterion is a metric relating vorticity magnitude and the shear strain rate. The vortices are then defined as areas where the former prevails over the latter. The analysis was done in ~25 setup time steps, and then continued for 5000 time steps, resulting in 0.1 seconds of analyzed flow.

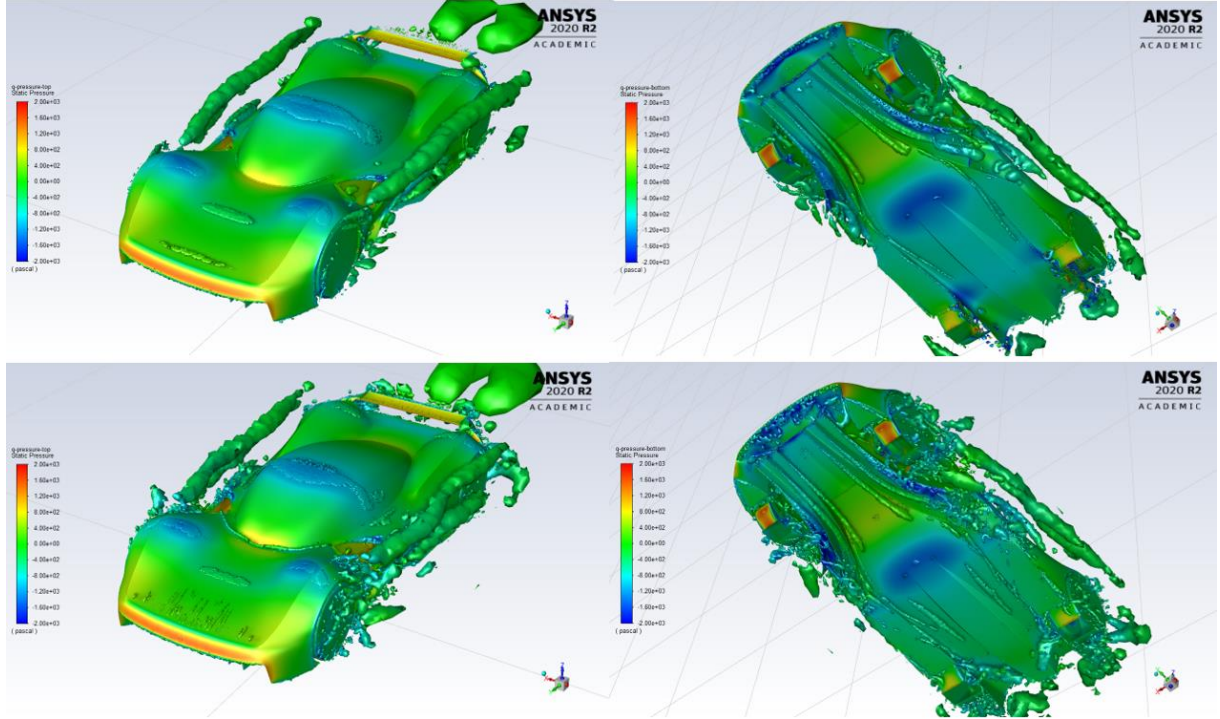


Figure 49: Pressure contour plots over geometry with Q-criterion=0.1 iso-surfaces added, taken at the start of the analysis and after 1000 2e-5 s time steps.

While Figure 49 provides interesting insight into difference between steady and transient results, important observations can be drawn from the flow in the latter half of the observation (Figure 50). It is interesting to see that the flow's behavior started showing periodic patterns, and while the top surface was shedding tiny vortices around the front separation area and bottom edge of the roof canopy, the vortices forming the longest vortex underneath the car started spontaneously combining and separating. This shows that the car would probably perform even worse in more detailed transient analysis.

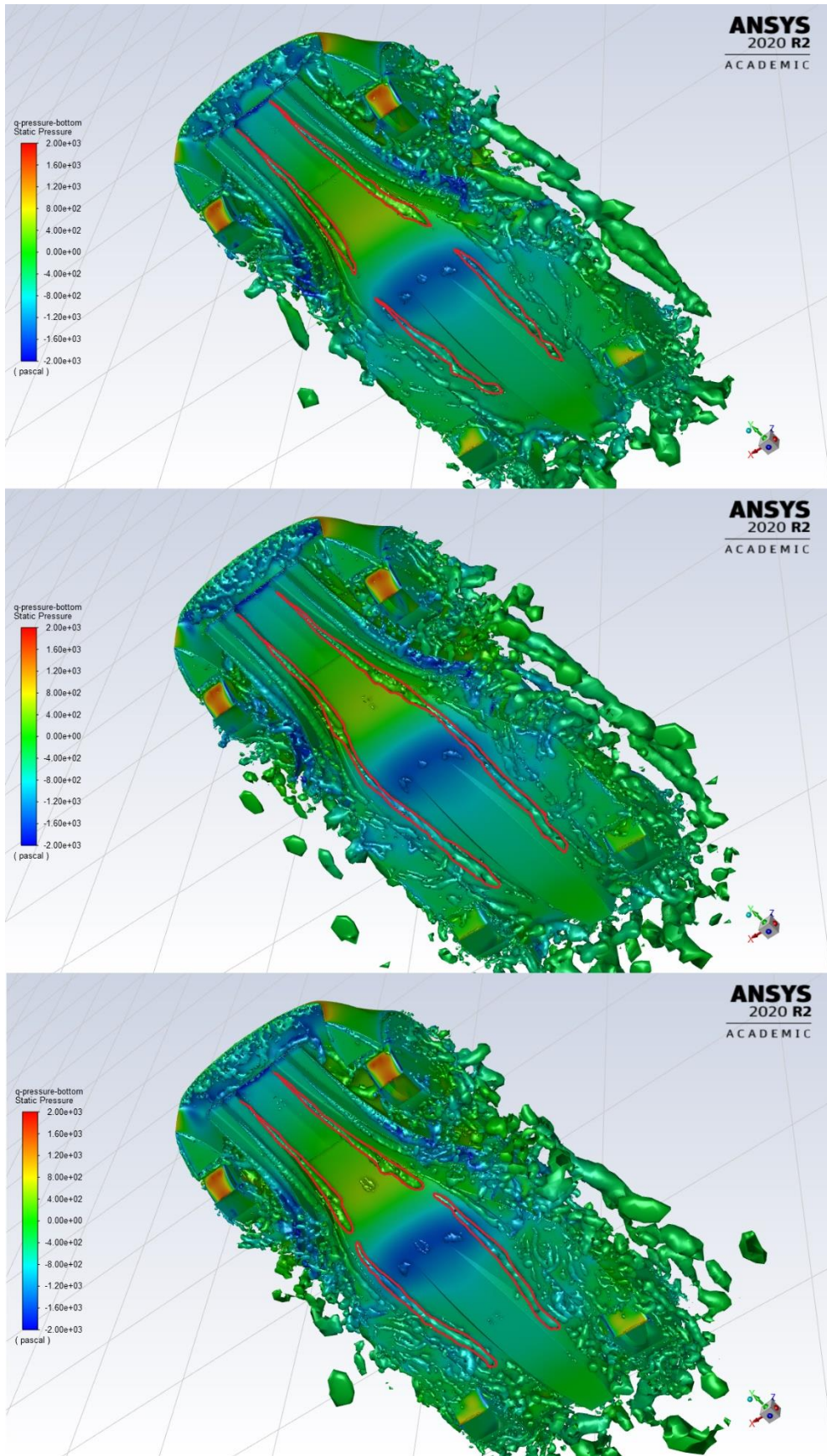


Figure 50: The same plots as in Figure 49, but at 2000, 3000 and 4185 time steps. Periodic behavior of the main vortex was outlined.

6. Conclusions

Performance-wise, there are several major problems in car's design which lead to its poor coefficient values. First and foremost, the front face of the car generates early separation leading to the turbulent flow going both over and under the rest of the car. The front wheel arches do not guide nor control the wake of the front wheels accurately enough, leading to the loss of downforce in front and rear tunnels. This could have been fixed with different shape of the arches behind the front wheels and extending the floor to shield rear parts of the front tunnels from below. The internal flow in the front of the car, while providing some downforce, also creates a large spot of positive pressure between the two largest area of negative pressure. This could have been avoided by either removing the front horizontal surface, sealing the opening behind it and/or creating additional outlets to remove high pressured air from this area. Also, the outlet of the front internal flow in front of the side radiators was a major cause of loss of function of front wheel arch pressure outlets. This could have been fixed by placing those outlets further away from each other. Moving along, curved footplates on the side floor extensions could have reduced amount of lateral flow disrupting the flow in the rear tunnels. The shape of the rear tunnels was also not prepared for the vortices coming from the front aerodynamic devices. This, and lack of the footplates on the outer edges of the tunnels, led to the large, uncontrolled vortices generated by the rear wheel wake. Another way of reducing rear wheel wake could have been longer lateral extensions at the end of the rear tunnels. The rear wing was too close to the rest of the bodywork, what both hurt its performance and reduced its influence on the diffuser. Finally, the bodywork itself has several intentional (aesthetic) and unintentional (geometry quality) areas, where unnecessary drag is being created. Overall, the car of this type usually generates a significant amount of negative pressure on its upper surfaces (and this one especially does, due to two-seat cockpit), and the negative pressure generated underneath the car is not enough to counteract this behavior strongly enough to create larger downforce. Also, the front of the car and largely uncontrolled wake created by front and rear wheels create significant drag.

The lesson from the design part of the project should also be noted; that of the importance of having a high-quality CAD model. It allows for faster fixes, allows for further design optimizations and leads to error-free meshing, which in turn improves analysis stability and results. Majority of the time spent on this project, including overrun deadlines, was spent on modeling.

Bibliography

1. *1/24 TOYOTA GAZOO Racing TS050 HYBRID 2019*. [Online]
Available at: <https://www.tamiya.com/english/products/25421/index.htm>
2. *Aston Martin Media*. [Online]
Available at: <https://media astonmartin.com/>
3. *Toyota TS050 Hybrid '2017*. [Online]
Available at:
https://en.wheelsage.org/toyota/ts/toyota_ts050_hybrid_2/2017/pictures/rusvqq
4. Katz, J., 2003. *New Directions in Race Car Aerodynamics: Designing for Speed (Engineering and Performance)*. s.l.:Bentley Publishers.
5. Keszeli, M., 2019. *F1 2021 wind tunnel model in 50% scale*. [Online]
Available at: <https://twitter.com/techf1les/status/1164593006894362625>
6. McBeath, S., 2017. *Competition Car Aerodynamics*. s.l.:Veloce Publishing Ltd..
7. Padeanu, A., 2016. *Elemental Rp1 generates 882 lbs of downforce at 150 mph*. [Online]
Available at: <https://www.motor1.com/news/64125/elemental-rp1-generates-882-lbs-of-downforce-at-150-mph/>
8. Piechna, J., 2000. *Podstawy aerodynamiki pojazdów*. s.l.:Wydawnictwa Komunikacji i Łączności.
9. Piola, G., n.d. *How a mistake helped create an F1 icon*. [Online]
Available at: <https://www.giorgiopiola.com/blogs/articles/how-a-mistake-helped-create-an-f1-icon>
10. Ruhrmann, A. & Zhang, X., 2003. Influence of Diffuser Angle on a Bluff Body in Ground Effect. *Journal of Fluids Engineering*.
11. Smale, G., n.d. *Porsche 956/962 remembered*. [Online]
Available at: <https://www.porscheroadandrace.com/porsche-956-962-remembered/>
12. Somerfield, M. & Piola, G., 2020. *Banned: The full story behind Brabham's F1 'fan car'*. [Online]
Available at: <https://www.motorsport.com/f1/news/banned-tech-brabham-bt46b-fan/4808234/>

List of figures

Figure 1: 1978 Brabham BT46B, the second and final fan-based ground effect race car [8] ..	6
Figure 2: Lotus 78 (top) and 79 (bottom). While 78 was technically a working implementation of the ground effect sidepods, Lotus did not win a championship with ground-effect car before using much-upgraded 79 [5]. ..	7
Figure 3: Early Porsche 956 aerodynamic model with deep Venturi tunnels visible [7].....	7
Figure 4: 2022 F1 regulations reference aerodynamic scale model. The new tunnels are white. [2] ..	8
Figure 5: Elemental RP1 underfloor.....	9
Figure 6: Aston Martin Valkyrie. Visible multi-element front wing and deep tunnels spanning most of the car's length.....	9
Figure 7: Initial whiteboard drawing with 2D human dummy.....	10
Figure 8: Final design drawing	11
Figure 9: Top surfaces of the front tunnels lead air to the side radiators.	12
Figure 10: Car's final underfloor design.....	12
Figure 11: Wheel well pressure outlets highlighted.	13
Figure 12: Internal tunnels for cooling system simulation.	13
Figure 13: After initial analysis, a surface connecting front tunnels was added.	14
Figure 14: Initial and final versions of tub and front tunnels.....	15
Figure 15: The final geometry with smooth edges hidden.	16
Figure 16: The final geometry with all edges shown. Having many edges and surfaces, some of which were small, caused multiple problems with mesh generation later in the process. .	16
Figure 17: Mesh overview with visible cell edges and boundary conditions (symmetry in brown and velocity-inlet in green).....	17
Figure 18: Detailed picture of the surface mesh on car's body and wheels.	18
Figure 19: A close-up image showing boundary layer mesh on both floor and front tunnels. It should be noted that all thin surfaces used in the model have thickness set to 5 mm.	18
Figure 20: A close-up image showing denser mesh on the car's rear wing.	19
Figure 21: Values of CL and CD depending on the surface mesh density. For plot clarity, the sign of CL was flipped. The car produces negative lift.....	20
Figure 22: Values of $y+$ over the car's body and wheels.	20
Figure 23: Significant pressure buildup on the front face, and a smaller one on the cockpit canopy. Large areas of negative pressure over the fender and the roof should can also be seen.....	21
Figure 24: A smaller pressure buildup on the end of the cockpit canopy.....	22
Figure 25: Large areas of negative pressure, combined with an area of positive pressure between them.	22
Figure 26: The large negative pressure area on the bottom of the wing would have been used better, if the wing were placed beyond the engine cover.	23
Figure 27: Surface of static pressure equal to zero indicating a bubble of high pressure being generated on the car's nose.....	23
Figure 28: More pressure bubbles are forming on a windshield, side outlets and around the rear wing.....	24
Figure 29: A small teardrop-shaped buildup of pressure in front of the rear fender is caused by the fault in the mesh (end of a sharp edge).	24
Figure 30: qualitative plot of pressures around the car's body.....	25

Figure 31: XY plot with scaled pressure values added over the car's surface. Blue areas represent negative pressure and orange represent positive. The shades only help visualize overlay of those areas.....	25
Figure 32: Major vortices shed from the top of the front wheels and minor from the bottom.	26
Figure 33: Limiting pathlines to only those starting from the front wheels confirms that the front wheels are responsible for two large vortices on each side of the car.	26
Figure 34: Front wheel wake seen from the bottom. It should be noted that the turbulent flow enters the front tunnels, and then later the rear tunnels as well.....	27
Figure 35: Toyota TS050 front diffuser inlet and exit.	27
Figure 36: Constant-color pathlines seen from the back. While rear wheel outlets seem to be working properly (top), the front wheel outlets seem to be feeding the vortex shed from the top of the front wheels.....	28
Figure 37: Plot of positive Y-velocity showing areas of reversed flow in vicinity of the rear tunnels.	28
Figure 38: Closeup on the rear of the car, seen from the bottom. Pathlines colored by Y-velocity (left) and by their source surface's ID for comparison (right). Reversed flow is the area in yellow.....	29
Figure 39: Aston Martin Valkyrie rear diffuser exit with detailed side extensions and bottom edge.....	29
Figure 40: Velocities are as expected knowing pressure distributions, but the flow in the rear tunnels suggests problems with vortex generation.	30
Figure 41: Vorticity contours on several planes. Note: Vorticity plots are symmetrical due to the fact that only "half" of the flow was simulated.	30
Figure 42: Vorticity in the rear tunnels starts only around the rear axis. Also, flow around the edge of the side floor extensions should be noted.....	31
Figure 43: Aston Martin Valkyrie side floor extension footplates.....	31
Figure 44: Helicity plot showing vortices progression down the flow. Note: like with the vorticity contours, only the left side of the car has correct values.	32
Figure 45: Helicity-colored pathlines (left) and source surface ID-colored pathlines for reference (right).	32
Figure 46: Oil flow visualization of the car's floor. No influence of vortices is visible on the surface of the rear tunnels.	33
Figure 47: Total pressure losses. Front wheel wake seems to produce a lot of drag except reducing downforce.....	34
Figure 48: Total pressure losses in the back. The losses start appearing around the back just where the rear wheel wake enters the rear tunnels.	34
Figure 49: Pressure contour plots over geometry with Q-criterion=0.1 iso-surfaces added, taken at the start of the analysis and after 1000 2e-5 s time steps.	35
Figure 50: The same plots as in Figure 49, but at 2000, 3000 and 4185 time steps. Periodic behavior of the main vortex was outlined.	36